Published in GSA Bulletin 117, issues 5-6, 589-619, 2005,
which should be used for any reference to this work

Phosphogenesis and organic-carbon preservation in the Miocene Monterey Formation at Naples Beach, California—The Monterey hypothesis revisited

Karl B. Föllmi[†]
Christophe Badertscher
Institut de Géologie, Université de Neuchâtel, CH-2007 Neuchâtel, Switzerland

Eric de Kaenel
DeKaenel Paleo-Research, CH-2000 Neuchâtel, Switzerland

Peter Stille
Centre de Géochimie de la Surface, Université Louis Pasteur, F-67084 Strasbourg, France

Cédric M. John[‡]
Thierry Adatte
Philipp Steinmann
Institut de Géologie, Université de Neuchâtel, CH-2007 Neuchâtel, Switzerland

ABSTRACT

The middle part of the Miocene Monterey Formation at Naples Beach, west of Santa Barbara, California, is predominantly composed of organic-rich mudstone interstratified with phosphatic laminae. Minor lithologies include volcanic ash, dolomite, porcelanite and chert, and condensed phosphatic beds. Sediments dated as 14.3–13.5 Ma have average total organic carbon (TOC) values around 8.5 wt%, and organic carbon (OC) accumulation rates are around 565 mg/cm^2/k.y. Sediments dated as 13.5–13 Ma are characterized by average TOC values of 12.6 wt% and OC accumulation rates of around 1130 mg/cm^2/k.y. The interval between 13 and 10.6 Ma is marked by condensation; average TOC values are around 8.6 wt%, and OC accumulation rates diminished to around 55 mg/cm^2/k.y. The last interval studied is dated as 10.6–9.4 Ma, and average TOC values are around 6 wt%, whereas OC accumulation rates rose again to 320 mg/cm^2/k.y.

The presence of erosional surfaces, angular unconformities, and reworked clasts and nodules suggests that bottom-current activity and gravity-flow deposition have been instrumental in sediment accumulation. The phosphatic laminae were precipitated at a very early stage of diagenesis during periods of nonsedimentation. They formed less permeable sedimentary lids and may as such have contributed to enhanced OC preservation. Between 13 and 10.6 Ma, the thus-formed phosphatic laminae were frequently subjected to subsequent sediment winnowing and reworking, resulting in the formation of condensed phosphatic beds. Calculated P:C molar ratios suggest that (1) the measured section is highly enriched in phosphorus (P) relative to OC; (2) regeneration of organic P from organic-matter decomposition was negligible; and (3) the source of P was external, likely upwelled bottom water rich in inorganic P.

In spite of good preservation conditions and correspondingly high TOC contents, the overall OC accumulation rates are moderate in comparison to those of actual high productivity areas, which is mainly due to the episodic character of depositional processes and the intervening long periods of nondeposition and sediment reworking. They preclude this section, and by extrapolation, the Monterey Formation in general from being an important OC sink during the middle Miocene. Alternatively, large OC sinks were probably created on the continent (lignite deposits) and in sedimentary depocenters, which received increasing amounts of detrital sediments due to a combination of climate change, spreading of grasslands, and the increasing importance of mountain chains such as the Himalaya. The associated high nutrient fluxes may have been involved in the backstepping and drowning of carbonate platforms and in the generation of widespread phosphate-rich deposits during the late early and early middle Miocene.

Keywords: Monterey Formation, Naples Beach, organic carbon preservation, phosphogenesis, Monterey hypothesis, Miocene.

INTRODUCTION

The middle to upper Miocene Monterey Formation of the central Californian coastal area consists of a unique hemipelagic to pelagic succession, which comprises sediments rich in organic matter, carbonate, phosphate, and biosilica, and their diagenetic derivatives such as porcelanite and chert (Bramlette, 1946; Garrison and Douglas, 1981; Isaacs and Garrison, 1983; Isaacs and Peterson, 1987; Barron, 1986a; MacKinnon, 1989; Hornafius, 1994; Kunitomi et al., 1998; Galloway, 1998; Behl, 1999; Chaika and Williams, 2001; Isaacs and Rullkötter, 2001). Many researchers have investigated this succession for a wide variety of studies including

[†]E-mail: karl.foellmi@unine.ch.
[‡]Present address: Department of Earth Sciences, University of California, Santa Cruz, California 95064, USA.

sedimentary and mineralogical composition, history of deep burial and subsequent uplift in an active margin setting, economic importance as an oil source and reservoir rock, and relevance for our understanding of climate development during the middle and late Miocene. More specifically, it represents a model formation for such diverse studies as: (1) the accumulation and preservation of organic matter (e.g., Summerhayes, 1981; Isaacs, 1981b, 1984, 1985, 2001; Isaacs and Peterson, 1987; Isaacs et al., 1983; Piper and Isaacs, 2001; Pisciotto and Garrison, 1981; John et al., 2002); (2) the origin and genesis of dolomite (e.g., Baker and Kastner, 1981; Garrison et al., 1984; Burns and Baker, 1987; Compton, 1988; Malone et al., 1994); (3) the transformation of opal A to opal CT and quartz (e.g., Murata and Randall, 1975; Pisciotto, 1981; Isaacs, 1981a, 1981b, 1981c, 1982; Keller and Isaacs, 1985; Compton, 1991a; Behl, 1992; Behl and Garrison, 1994); (4) phosphogenesis (e.g., Garrison et al., 1987, 1990, 1994; Reimers et al., 1990; Föllmi and Garrison, 1991; Föllmi et al., 1991; Kolodny and Garrison, 1994; Medrano and Piper, 1997; John et al., 2002); (5) clay-mineral transformations (e.g., Compton, 1991b); (6) bio-, magneto-, and chemostratigraphy (e.g., Kleinpell, 1938, 1980; Ingle, 1980; Blake, 1981, 1994; Vincent and Berger, 1985; Arends and Blake, 1986; Barron, 1986b; Barron and Isaacs, 2001; De Paolo and Finger, 1991; White, 1992; White et al., 1992; Khan-Omarzai et al., 1993; Flower and Kennett, 1993, 1994a; Echols, 1994); (7) paleoecology (e.g., Föllmi and Grimm, 1990); (8) geochemistry (e.g., Filippelli and Delaney, 1992, 1994; Filippelli et al., 1994); (9) postdepositional deformation and fracturation (e.g., Seilacher, 1969; Gross, 1995; Grimm and Orange, 1997; Eichhubl and Boles, 2000); and (10) structural and tectonic development of the depositional environment (e.g., Graham and Williams, 1985; Graham, 1987; Hoppie and Garrison, 2001, 2002).

One of the most intensively studied sections of the Monterey Formation is the section at Naples Beach, ~25 km W of Santa Barbara (Fig. 1; e.g., Isaacs, 1981b, 2001; Arends and Blake, 1986; MacKinnon, 1989; Blake, 1994; Flower and Kennett, 1993, 1994a; Garrison et al., 1994; Hornafius, 1994; Grimm and Orange, 1997; Badertscher, 2000). This section is outstanding with regard to its quality of exposure, continuity, and lithological diversity and is regarded as a classical type locality for the Monterey formation (e.g., Hornafius, 1994), which depositional environment has been associated with a low-gradient slope (Isaacs, 2001). In spite of the multitude of studies performed on this section, several aspects remain controversial or poorly understood: (1) Age control has been obtained using diatom biostratigraphy (Barron, 1986b; Barron and Isaacs, 2001), benthic foraminifer biostratigraphy (Kleinpell, 1980; Arends and Blake, 1986; Blake, 1994), and strontium isotope stratigraphy (De Paolo and Finger, 1991). The ages assigned to this section and especially to its central, organic- and phosphate-rich succession are, however, not entirely compatible and are in need of improvement. Good age control is relevant for correlation purposes, calculation of accumulation rates, and last but not least for the verification of the Monterey hypothesis (Vincent and Berger, 1985), by which a causal relationship is claimed between middle Miocene climate cooling and the preservation of organic carbon in the Monterey and related formations (see also Raymo, 1994; John et al., 2002). (2) A second challenge is the development of a model of sediment accumulation and organic matter preservation, which is compatible with the calculated low sediment accumulation rates (Isaacs, 2001; John et al., 2002) and observed sedimentological and early diagenetic structures. This is relevant to the discussion whether deposition occurred in a slow and continuous fashion, characterized by particle by particle deposition (e.g., Hoppie and Garrison, 2002) or in a more episodic fashion (e.g., Föllmi and Garrison, 1991; Chang and Grimm, 1999). (3) A third challenge remains the deciphering of the conditions that led to the genesis of the close and regular juxtaposition of organic and phosphate-rich sediments, a combination that requires rapid and regular change in depositional and early diagenetic conditions.

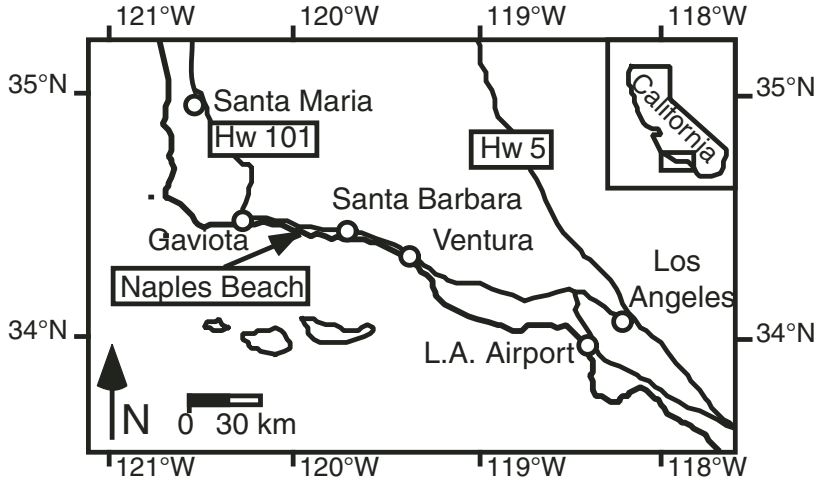

Figure 1. Location of the section at Naples Beach.

Here we present a detailed stratigraphic log of the central part of the Monterey section at Naples Beach, which is rich in organic matter and phosphate. We propose a new age model for this succession based on calcareous nannofossil biostratigraphy and present a model for the accumulation and preservation of organic- and phosphate-rich sediments for this locality. Last but not least we discuss the new age and accumulation data obtained during this study (Badertscher, 2000) and a related study by John et al. (2002) in the light of the Monterey hypothesis.

ANALYTICAL METHODS

The section at Naples Beach was measured in detail and sampled with a density of ~1 sample per 2 m for its lower and upper part and ~2 samples per meter for its middle part rich in organic matter and phosphates (Fig. 2). The thus-obtained samples were cleaned and cut perpendicular to bedding. One sample half was polished and the other half was used to make thin sections and sample powders. We used Rock-Eval™6 (temperature ranges for pyrolysis and oxidation: 300–650 °C and 400–850 °C, respectively; heating steps 25 °C/min; initial time 3 min; Espitalié et al., 1985; Behar et al., 2001) for the analysis of total organic carbon (TOC), hydrogen index, and T_{max}. For determination of the mineral composition of bulk samples, a Scintag XRD 2000 diffractometer was employed following the methods described by Kübler (1983) and Adatte et al. (1996). Slides for nannoplankton identification were made using the settling method described in De Kaenel and Villa (1996). A selection of samples was imaged using scanning electron microscopy (SEM; Philips XL20) and environmental scanning electron microscopy equipped with an energy dispersive spectrometer (ESEM-EDS; Philips XL30 FEG). Phosphorus (P) contents and phases were identified using a sequential extraction method (Ruttenberg, 1992; Filippelli and Delaney, 1996; Anderson and Delaney,

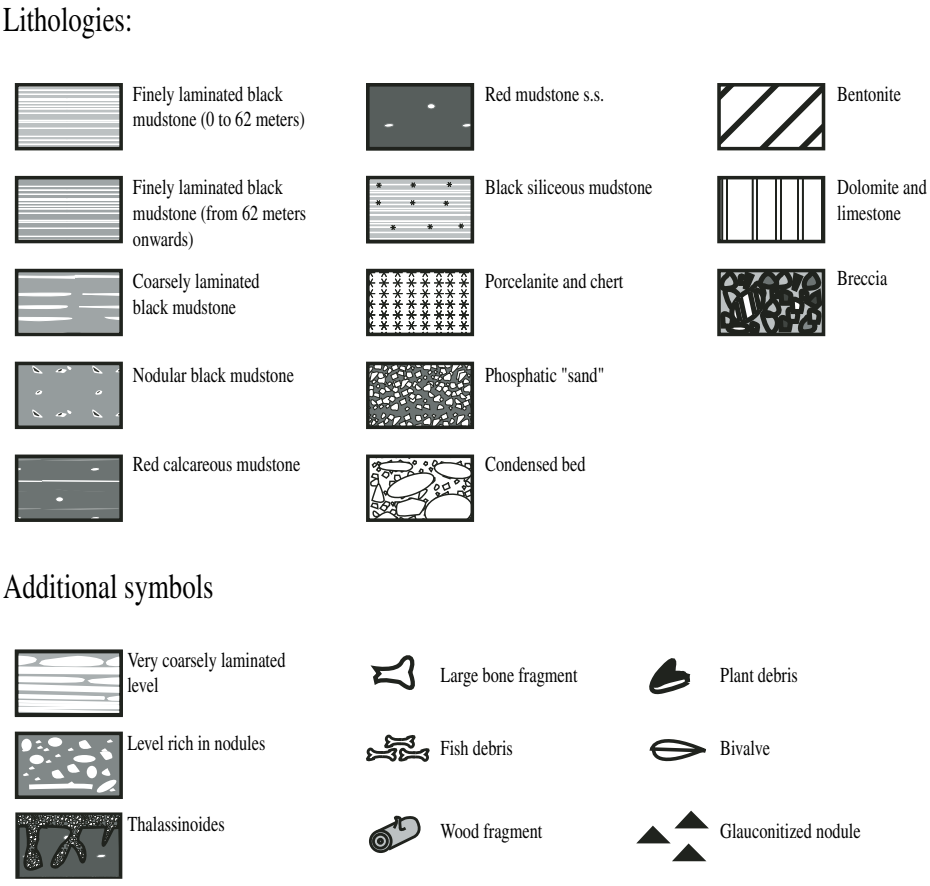

Figure 2. Detailed log of the measured section at Naples Beach, which covers the middle, carbonaceous and phosphate-rich member of the Monterey Formation (adapted from Badetscher, 2000). Section starts at the east side of the Dos Pueblo Canyon. Note the change in scale at 60 m and 108 m. Note also that the limits between the different mudstone types are often transitional. Sample identification is NB (Naples Beach) + number (samples were taken in 1987), Nap (Naples) + number (samples were collected in 1998), and Dat (Dating) + number (samples were taken for the purpose of calcareous nannofossil dating in 1999). **(*Continued on following three pages.*)**

2000; Tamburini, 2001). A selection of phosphates was analyzed for strontium isotopes at the Centre de Géochimie de la Surface (CNRS) in Strasbourg, France, using a fully automated VG Sector mass spectrometer and the preparation methods and correction factors in Stille et al. (1994).

STRATIGRAPHY

The Monterey Formation overlies a series of clayey mudstone containing dolomite concretions that belong to the Rincon Formation (e.g., Hornafius, 1994). The formation itself starts with an ~200-m-thick succession of siliceous mudstone, which is topped by a prominent interval of synsedimentary reworking (slump folds, breccias) immediately west of the Dos Pueblos Creek. At the eastern side of the Dos Pueblos Creek, the section continues with an ~180-m-thick succession of calcareous and siliceous mudstone rich in organic matter and phosphate, which contains a series of condensed phosphatic beds that were measured and sampled for this study (Fig. 2). The upper portion of the Monterey Formation consists of ~100 m of siliceous mudstone. The contact to the overlying Sisquoc Formation is marked by erosion and the clayey siliceous mudstone of this formation includes several intervals with reworked sediments of the Monterey Formation.

We distinguish the following lithologies in the measured section (Fig. 2 and Table 1). (1) Finely laminated black mudstone: a dark-colored mudstone characterized by the regular occurrence of light-colored phosphatic laminae, which are laterally mostly continuous. (2) Coarsely laminated black mudstone: the coarse phosphatic laminae are laterally discontinuous. (3) Nodular black mudstone: this lithology includes frequent phosphatic particles and nodules; phosphatic laminae are less abundant. (4) Red mudstone: granular phosphatic layers and isolated phosphatic nodules are frequent in this lithology, whereas phosphatic laminae are not as abundant. Calcareous benthic foraminifera are rare and agglutinated benthic foraminifera are very common. The rusty red to brown color is probably due to surficial oxidation of iron-containing minerals. (5) Siliceous mudstone: this type of mudstone is similar to black mudstone except for an increase in biosilica. (6) Phosphatic condensed beds: these horizons, which are up to 30 cm thick, are build up of phosphatic laminae, particles, and pebbles, which are commonly embedded in a phosphatic matrix. (7) Chert and porcelanite: some rare horizons within the siliceous mudstone consist of porcelanite and chert. (8) Dolomite and limestone: dolomite and limestone occur in discrete nodules and layers within the mudstone and phosphatic condensed beds. And (9) bentonite: volcanic ash layers are abundant in the measured section. They are normally millimeters thick but may attain bed thicknesses of up to 10 cm.

The here distinguished lithologies correlate well with the nearby section at El Capitan State Beach (John et al., 2002), the difference being that the black mudstone is differentiated here in three subtypes and that the gray mudstone described from the section at El Capitan State Beach and also characteristic for the lower part of the Monterey Formation at Naples Beach is not covered in the section described here.

CALCAREOUS NANNOFOSSIL BIOSTRATIGRAPHY

Different age models have been proposed for the Monterey Formation, which for a large part have been derived from the section at Naples Beach. These models are based on biostratigraphy (benthic foraminifera: Kleinpell, 1938, 1980; Arends and Blake, 1986; Blake, 1994; diatoms: Barron, 1986b; Barron and Isaacs, 2001), strontium isotope stratigraphy (De Paolo and Finger, 1991), and magnetostratigraphy (Khan-Omarzai et al., 1993). With regard to the condensed interval at Naples Beach, different age ranges have been postulated: Arends and Blake (1986) and Blake (1994) envisaged a time span of 14.8–9.3 Ma for its formation; Barron (1986b) and Barron and Isaacs (2001) estimated a period of 14.3–10.3 Ma; De Paolo and Finger (1991) proposed 14.8–13.7 Ma; and Khan-Omarzai et al. (1993) postulated 14.3–13.25 Ma for a correlatable condensed interval in the Monterey Formation at Shell Beach, south of

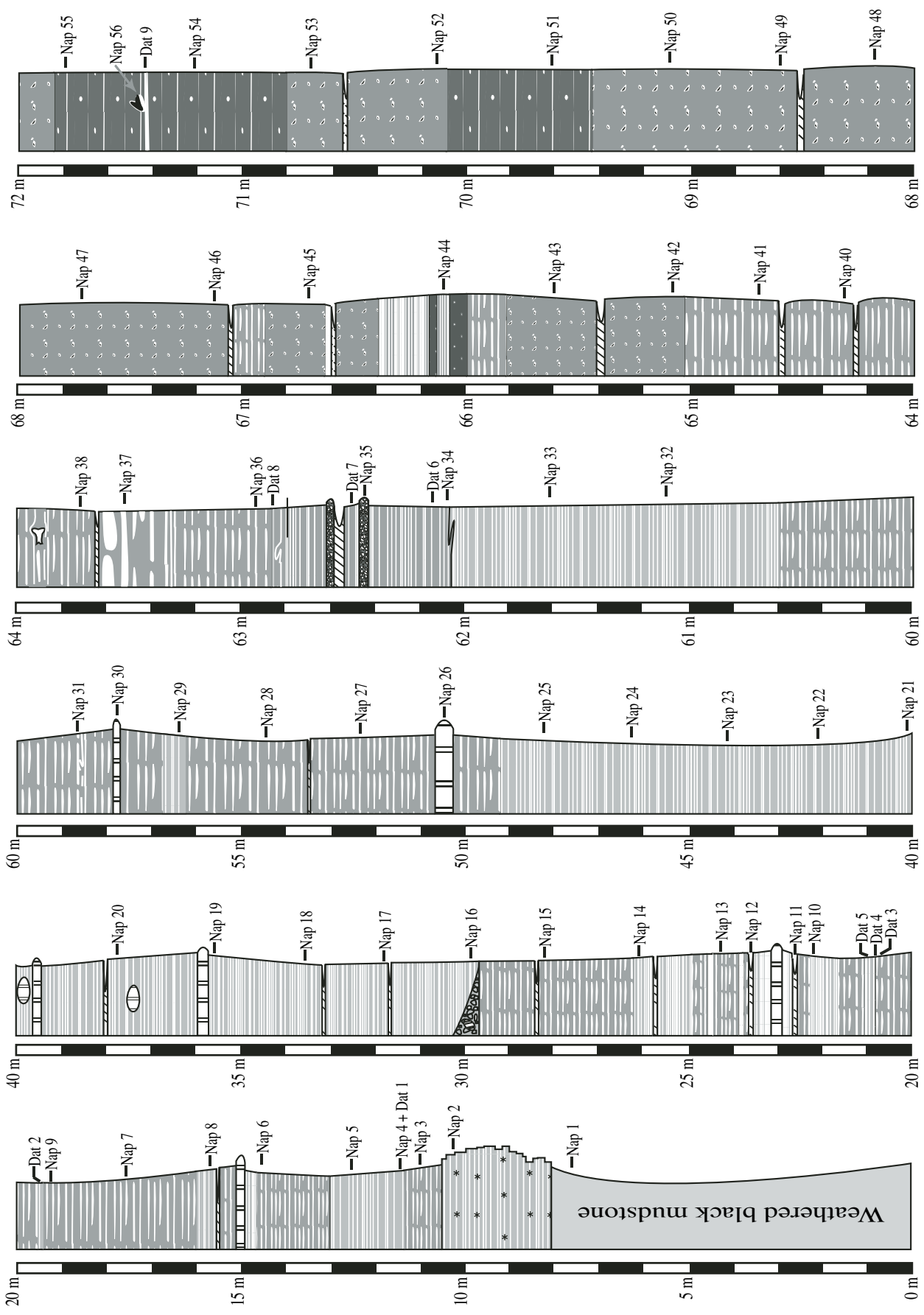

Figure 2 (*continued*).

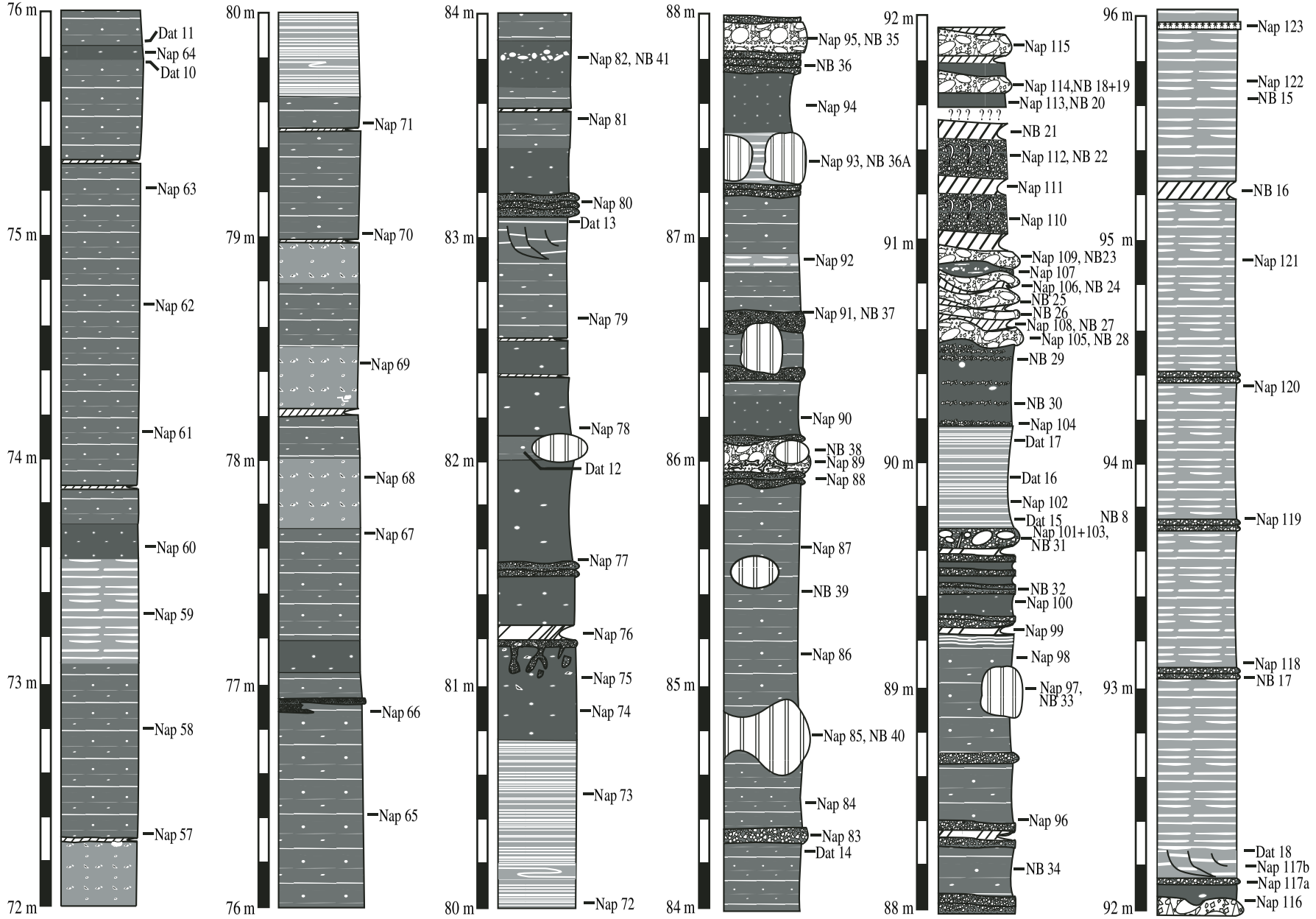

Figure 2 (*continued*).

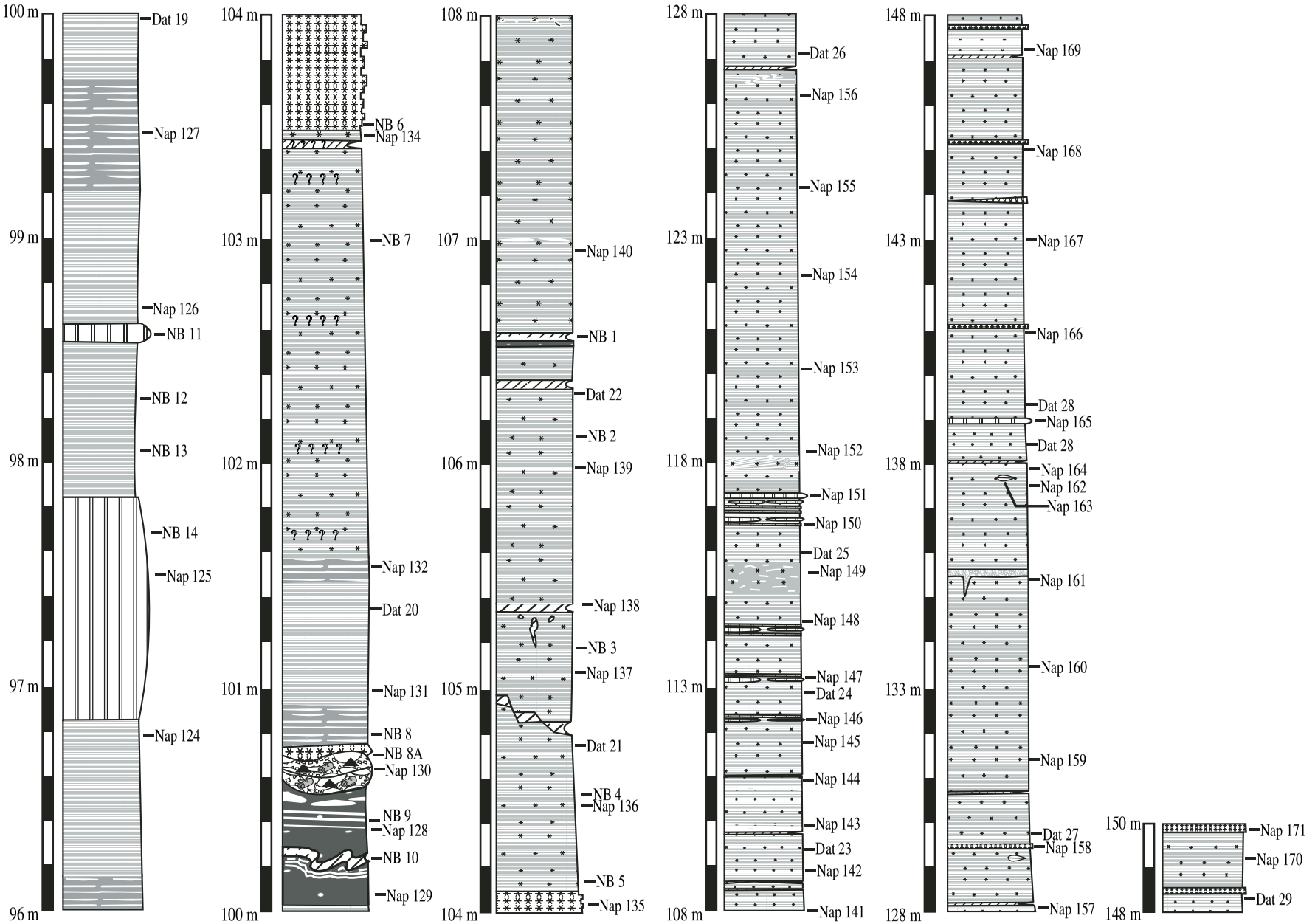

Figure 2 (*continued*).

TABLE 1. AVERAGE, MINIMAL, AND MAXIMUM VALUES FOR MAJOR MINERALS OF THE DIFFERENT LITHOLOGIES DISTINGUISHED IN THE MEASURED SECTION (FIG. 2) IN WEIGHT PERCENT

Sample number	Carbonate fluor-apatite	Phyllosilicate	Quartz and feldspar	Calcite	Ankerite	Total organic carbon
Black mudstone, finely laminated						
22	4.10 (0–7,67)	9.56 (1,91–18,95)	5.80 (2,36–14,06)	46.58 (27,58–62,57)	0.37 (0–4,67)	7.42 (3,43–11,37)
Black mudstone, coarsely laminated						
24	10.13 (7,43–16,77)	11.18 (4,72–15,24)	10.04 (3,93–17,5)	17.73 (0–34,55)	0.00	11.09 (6,82–15,22)
Black mudstone, nodular						
11	4.76 (2,03–7,04)	10.88 (6,87–15,65)	7.58 (4,51–9,62)	26.60 (17,31–38,61)	0.06 (0–0,34)	12.32 (9,24–15,22)
Black mudstone, siliceous						
24	3.69 (0–7,69)	14.74 (7,85–23,96)	11.65 (4,91–24,4)	16.50 (0–55,44)	0.24 (0–2,24)	6.25 (3,22–8,59)
Red mudstone, with carbonate						
15	2.22 (0–5,59)	15.12 (10,3–23,09)	10.61 (5,54–20,21)	19.52 (4,29–33,13)	0.09 (0–0,59)	15.59 (11,58–21,88)
Red mudstone, s.s.						
8	1.29 (0–3,89)	22.45 (18,28–28,45)	16.95 (13,03–20,89)	1.73 (0–7,79)	0.00	19.57 (16,53–22,17)
Granular phosphate						
6	42.50 (28,96–64,24)	6.87 (0–13,15)	12.08 (3,37–16,02)	8.90 (0–27,1)	0.00	6.17 (2,6–8,25)
Condensed horizons						
9	51.86 (29,15–78,48)	3.09 (0–27,8)	3.14 (1,28–7,74)	0.00	0.00	1.60 (0,75–2,62)
Dolomite and limestone						
13	0.93 (0–4,74)	0.00	1.49 (0–4,12)	34.33 (5,48–94,57)	20.73 (0–34,48)	1.68 (0,24–2,9)
Bentonite						
7	0.60 (0–4,22)	14.62 (0–48,34)	4.97 (0,94–19,58)	1.22 (0–6,69)	0.00	0.17 (0,07–0,35)

San Luis Obispo (compare also Khan-Omarzai et al., 2001).

Here we propose a new age model for the central portion of the Monterey Formation, which is based on the detailed analysis of preserved calcareous nannofossils in 49 samples, selected for their relatively high carbonate contents detected by systematic XRD screening of all collected samples. Table 2 gives a compilation of the identified nannofossil distributions and Table 3 contains a summary of calcareous nannofossil events and corresponding ages, which have been calibrated against orbitally tuned time scales (Hilgen et al., 2000). Additional information on zonal schemes and calcareous nannofossil events is published in John et al. (2002).

Seventeen age dates result from this analysis (Fig. 3), pointing to a time interval between 13.5 and 13 Ma for the deposition of red mudstone and between 13 and 12 Ma for the formation of the condensed interval (Dat 17 to Nap 124; Fig. 2). A second condensed bed just above the condensed interval is bracketed between 10.9 and 10.6 Ma (Nap 124 to Dat 20; Fig. 2).

The nearby section at El Capitan State Beach has also been dated by calcareous nannofossils (John et al., 2002) and we observe a good correlation in time for the different lithologies, with the exception of the condensed phosphatic beds. The formation of the condensed beds started at 12.7 Ma at El Capitan State Beach and at 13 Ma at Naples Beach. The youngest condensed phosphatic beds date as 10.8 Ma (El Capitan State Beach) and 10.6 Ma (Naples Beach). The entire intervals of low sedimentation rates are quite well correlated between both sections (between 13.3 and 10.8 Ma for the section at El Capitan State Beach and 13 and 10.6 Ma for the section at Naples Beach); within these intervals, however, the bulk of the condensed phosphatic beds appears near the base at Naples Beach, leaving a mudstone interval of ~8.5 m between the stack of condensed phosphatic beds (Nap 88 to Nap 116; Fig. 2) and the highest phosphatic condensed bed (Nap 130; Fig. 2), whereas at El Capitan State Beach, they appear near the top and have a mudstone interval at the base of the condensed interval.

MINERALOGICAL AND GEOCHEMICAL ANALYSES

XRD Analyses

We performed XRD analyses on 172 samples in order to study the mineral distribution and its evolution through time (Table 1 and Fig. 3). Phyllosilicates vary around 10 weight % (wt%) in black mudstone and around 15 wt% in red and siliceous mudstone. Measured phyllosilicates consist mainly of biotite and smectite, as in the nearby section at El Capitan State Beach. Quartz and feldspar contents vary between 5 and 15 wt%. Since porcelanite and chert are rare lithologies in the measured section and most biosiliceous material is still present as opal CT (Isaacs, 1981a; Isaacs et al., 1983; Behl, 1992), the quartz phase measured here is mostly of detrital origin. Calcite contents are quite variable and amount to an average of almost 50 wt% in the finely laminated black mudstone. They diminish in the coarsely laminated, nodular, and siliceous mudstone and become very low in the red mudstone (average around 1.73 wt%; Table 1). The calcite content is mostly related to the presence of foraminifera and calcareous nannofossils, which may partly form oozes (Table 2). Carbonate fluor-apatite (CFA) concentrations vary around 3.5–10 wt% in black mudstone, and diminish to 1.2–2.2 wt% in red mudstone. The condensed phosphatic beds contain up to 78 wt% CFA. Minor mineralogies identified include ankerite, dolomite, pyrite, and zeolite, and we identified jarosite, gypsum, and halite (sea-shore exposure) as secondary minerals.

Rock-Eval Analyses

We systematically analyzed all samples for TOC contents using Rock-Eval. Black mudstone shows average TOC contents between 7 and 12 wt%, whereas red mudstone has an average TOC content of ~15 wt%. Siliceous mudstone shows an average TOC content of ~6 wt% (Table 1).

A hydrogen index versus T_{max} cross plot (Fig. 4) suggests a consistent affiliation of the analyzed organic matter with type II kerogen. Type II kerogen is usually associated with a marine origin (cf. Summerhayes, 1981; Isaacs and Petersen, 1987). Organic matter from the condensed phosphatic beds plots low within the type II kerogen field and partly within the type III kerogen field. Those samples are character-

TABLE 2. CALCAREOUS NANNOFOSSIL DISTRIBUTIONS IDENTIFIED IN THE STUDIED SECTION OF THE MONTEREY FORMATION AT NAPLES BEACH

Epoch	Stage	Nannofossil Zone	Age (Ma)	Calcareous Nannofossil Events	Total Abundance	Diversity	Sample ID	Sample Depth (meters)	Calcareous nannofossils abundances	Calcareous nannofossils preservation	Diatoms abundance	*Coccolithus crassipons*	*Coccolithus pelagicus*	*Coccolithus pliopelagicus*	*Coronocyclus aff. C. prionion*	*Coronocyclus nitescens* (ell.)	*Cyclicargo. abisectus* (>10)	*Cyclicargo. floridanus* (<9)	*Dictyococcites perplexus*	*Dictyococcites productus*	*Discoaster deflandrei*	*Discoaster variabilis*	*Geminilithella rotula*	*Hayella aperta*	*Helicosphaera ampliaperta*	*Helicosphaera carteri*	*Helicosphaera intermedia*	*Helicosphaera paleocarteri*
Late Miocene	Tortonian	NN10	9.36	LO D. pentaradiatus	4877	36	DAT29	150.40	OOZE	GOOD	ABUNDANT		A	A					R	V		F	R			P		
			9.39	LRO D. pseudovariabilis	329	23	168	147.00	ABUNDANT	POOR	ABUNDANT		F	C					P	R		R						
		NN9			255	5	DAT28	141.20	ABUNDANT	POOR	ABUNDANT		F	C														
					740	5	166	140.90	ABUNDANT	POOR	ABUNDANT		C	C														
					2125	13	160	133.50	OOZE	POOR	ABUNDANT		A	A								P				F		
					1121	18	DAT27	129.70	OOZE	POOR	ABUNDANT		A	R					R	R		R				P		P
					2245	22	DAT26	127.40	OOZE	POOR	OOZE		A	C						F			P			F		
			9.88	Increase M. convallis	4282	16	155	124.20	OOZE	MIXED	ABUNDANT		A	A						C		P				P		
					1866	23	153	120.20	OOZE	POOR	ABUNDANT		A	A								C				F		
			9.94	LO M. convallis	678	16	DAT25	115.90	ABUNDANT	POOR	OOZE		C	A					P	P		F				R		
			10.29	HRO H. intermedia	2347	25	DAT24	112.70	OOZE	POOR	ABUNDANT		C	A					R	A						R	R	
					3283	17	DAT23	109.60	OOZE	POOR	ABUNDANT		C	V						F		P				P	P	
			10.44	HO D. exilis	745	8	DAT22	106.50	ABUNDANT	POOR	ABUNDANT		A	C						P								
					146	10	DAT21	104.80	COMMON	POOR	COMMON		F	F								R						
			10.60	LO D. cf. D. bollii	1776	26	DAT20	101.30	OOZE	MODERATE	ABUNDANT		C	C					F	F		R				P		
Middle Miocene	Serravallian	NN7	10.91	LCO C. macintyrei (>11)	2960	25	DAT19	99.90	OOZE	MIXED	RARE		A	C					R	C		R				P	P	
		NN6	12.00	HO C. floridanus (<9)	2188	21	124	96.80	OOZE	MODERATE	COMMON		F	C				P		F	P	R						
					1018	5	DAT18	92.40	OOZE	MODERATE	ABSENT			A								P				P		
					45	11	117b	92.20	FEW	MODERATE	PRESENT			P							P					P		
					865	12	DAT17	90.10	ABUNDANT	MODERATE	ABSENT		C	A							R	F					P	
			12.57	HRO C. premacintyrei (>9)	1307	11	DAT16	89.95	OOZE	MODERATE	ABSENT		C	A					P		R	P						
			13.03	increase H. walbersdorfensis	5443	24	DAT15	89.70	OOZE	GOOD	ABSENT		C	A						F	F	P	F			C	C	F
			13.03	LO acme R. pseudoumbilicus (>8)	7582	23	102	89.70	OOZE	GOOD	ABSENT	R		C				P	R		P		P			A	A	C
			13.28	LCO R. pseudoumbilicus (>8)	5192	14	098	89.00	OOZE	MODERATE	ABSENT	R		A					P							C		R
				Shift dominance C. floridanus-R. pseudo.	1680	16	092	86.90	OOZE	POOR	ABSENT			A					P	C		P					R	
			13.31	HCO C. floridanus (<9)	1214	10	087	85.60	OOZE	MODERATE	ABSENT			C				F		F		A						
					4097	9	DAT14	84.20	OOZE	MIXED	ABSENT			A				A				A	P					
					2315	13	DAT13	83.10	OOZE	MODERATE	ABUNDANT		F	A				C		A		C				F		F
					822	11	DAT12	82.00	ABUNDANT	POOR	ABSENT			C				C			P	P				C		
						0	DAT11	75.90	ABSENT		ABSENT																	
					2192	12	DAT10	75.70	OOZE	MODERATE	ABUNDANT		C	A				C	R	A						R		R
						0	DAT9	71.40	ABSENT		ABSENT																	
					6808	9	053	70.70	OOZE	POOR	ABSENT			A				A								A		
					2109	9	DAT8	62.90	OOZE	MODERATE	ABUNDANT			A						A						A		F
					2865	16	DAT7	62.50	OOZE	MODERATE	ABUNDANT		A	A				F		C		F	C			A		
				HO D. petaliformis	2430	21	DAT6	62.20	OOZE	MIXED	ABUNDANT		C	A		P		R	R	A		F				A	C	C
		NN5	13.50	S. heteromorphus, C. floridanus (9-10)	4922	28	031	58.60	OOZE	MODERATE	ABUNDANT		A	A		P		C	R	C		R				C	P	
					4283	17	029	56.40	OOZE	MODERATE	ABUNDANT		A	A		P		F	R	F			R			C	P	C
			13.76	LO D. musicus	2110	10	025	48.20	OOZE	MIXED	ABUNDANT		C	A				F								F		
			13.99	LCO H. walbersdorfensis	13383	11	021	40.00	OOZE	MIXED	ABUNDANT			A				P	R	C			R			A		C
					4153	9	016	29.90	OOZE	MIXED	ABUNDANT			A				P		C						A		C
			14.26	HCO D. deflandrei	12778	14	DAT5	21.35	OOZE	MIXED	ABSENT			A		P		P			C	P				C	F	C
					13082	8	DAT4	21.20	OOZE	MIXED	ABSENT			A								R				A		
						0	DAT3	21.00	ABSENT	MIXED	ABSENT																	
					597	10	DAT2	19,9	ABUNDANT	POOR	ABUNDANT			A							P	F				C	P	
					625	7	006	14.50	ABUNDANT	POOR	ABSENT			A				C				F				F		
					501	2	DAT1	11.10	ABUNDANT	MIXED	ABSENT			A				P										
					3745	16	003	10.90	OOZE	MIXED	OOZE			A	R				P	R		R				C		P
	LANGHIAN	NN4	14.94	HO H. ampliaperta	6821	24	D4	(-30.00)	OOZE	GOOD	PRESENT	P	A	A	F	P	P	P	R	F	R	P	R	P	F	C	F

(*continued*)

Note: A—absent; P (present) = 1–2 specimens per 201–500 fields of view; R (rare) = 3–14 specimens, one specimen per 51–200 fields of view; F (few) = 15–74 specimens, one specimen per 11–50 fields of view; C (common) = 75–150 specimens, one specimen per 2–10 fields of view; A (abundant) = 151–1000 specimens, 1–10 per field of view; O (ooze) = 1001–5000 specimens, >10 specimens per field of view.

TABLE 3. SUMMARY OF NANNOFOSSIL EVENTS AND ESTIMATED AGES

Nannofossil zone	Standard biohorizons/secondary nannofossil events	Type event	Age (Ma)	Reference sections
NN10	*Discoaster bollii*	HO—highest occurrence	9.24	ODP Leg 154, Site 926
	Discoaster pentaradiatus	LCO—lowest common occurrence	9.36	ODP Leg 154, Site 926
NN9	*Discoaster hamatus*	HO—highest occurrence	9.57	ODP Leg 154, Site 926
	Minylitha convallis	LO acme—lowest acme occurrence	9.88	ODP Leg 154, Site 926
	Discoaster pentaradiatus	LO—lowest occurrence	9.88	ODP Leg 154, Site 926
	Minylitha convallis	LO—lowest occurrence	9.94	ODP Leg 154, Site 926
	Helicosphaera intermedia	HRO—highest regular occurrence	10.29	ODP Leg 154, Site 926
	Discoaster exilis	HO—highest occurrence	10.44	ODP Leg 154, Site 926
	Discoaster cf. *bollii* (long ray)	LO—lowest occurrence	10.60	ODP Leg 154, Site 927
NN9	*Discoaster hamatus*	LO—lowest occurrence	10.67	ODP Leg 154, Site 926
	Calcidiscus macintyrei (>11 μm)	LCO—lowest common occurrence	10.91	ODP Leg 154, Site 926
NN8	*Catinaster coalitus coalitus*	LO—lowest occurrence	10.92	ODP Leg 154, Site 926
	Discoaster deflandrei	HO—highest occurrence	11.54	ODP Leg 154, Site 926
NN7	*Discoaster kugleri*	LO—lowest occurrence	11.89	ODP Leg 154, Site 926
	Cyclicargolithus floridanus (<9 μm)	HO—highest occurrence	12.00	ODP Leg 154, Site 926
	Calcidiscus premacintyrei (>9 μm)	HRO—highest regular occurrence	12.57	ODP Leg 154, Site 926
	Helicosphaera walbersdorfensis	HRO—highest regular occurrence	12.57	ODP Leg 154, Site 926
	Helicosphaera walbersdorfensis	HCO—highest common occurrence	13.03	ODP Leg 154, Site 926
	Reticulofenestra pseudoumbilica (>8 μm)	LCO—lowest common occurrence	13.27	ODP Leg 154, Site 926
	R. pseudoumbilica (>8 μm) >*C. floridanus* (>9 μm)	X—crossover abundance	13.28	ODP Leg 154, Site 926
	Cyclicargolithus floridanus (<9 μm)	HCO—highest common occurrence	13.31	ODP Leg 154, Site 926
	Discoaster musicus	HO—highest occurrence	13.41	ODP Leg 154, Site 926
NN5	*Sphenolithus heteromorphus*	HO—highest occurrence	13.50	ODP Leg 154, Site 926
	Discoaster musicus	LO—lowest occurrence	13.77	ODP Leg 154, Site 926
	Helicosphaera walbersdorfensis	LRO—lowest regular occurrence	13.99	ODP Leg 154, Site 926
	Discoaster deflandrei	HCO—highest common occurrence	14.26	ODP Leg 154, Site 925
NN4	*Helicosphaera ampliaperta*	HO—highest occurrence	14.94	ODP Leg 154, Site 925

ized by low TOC contents (average is 1.6 wt%) and the included organic material may have been altered during the process of condensation.

Phosphate Analyses

In order to improve our understanding of pathways of phosphate transfer and phosphogenesis, we analyzed 16 selected samples using the Sedex method (Fig. 5; Ruttenberg, 1992; Filippelli and Delaney, 1996; Anderson and Delaney, 2000; Tamburini, 2001; compare Filippelli and Delaney, 1995, for a similar study on the Monterey Formation at Shell Beach, Pismo Basin). This method allows for the identification and quantification of organically bound, iron- and manganese-bound, detrital, and authigenic phosphorus (including phosphorus associated with fish debris, calcium carbonate, and smectite) phases.

In all lithologies, organic and iron- and manganese-bound phosphorus are subordinate phases relative to authigenic and detrital phosphorus. The detrital phosphorus phase does not correlate well with contents of detrital quartz and appears to be high in condensed and reworked samples with no macroscopic trace of detrital phosphorus. We concur with Filippelli and Delaney (1995) that the detrital phase may correspond to an authigenic phase, which has undergone subsequent recrystallization and fluor enrichment (see below; Shemesh, 1990). This would signify that the great majority of identified phosphorus phases classify as authigenic phosphorus.

The measurement of phosphorus contents in context with TOC contents allows us to calculate P:C molar ratios for a selection of five whole-rock samples (i.e., mudstone including phosphatic laminae): three finely laminated black mudstone samples obtained ratios of 1:28, 1:31, and 1:129, whereas two siliceous mudstone samples have ratios of 1:37 and 1:51. The detailed analysis of separate sediment and mineral phases within one coarsely laminated mudstone sample was particularly interesting. Two measurements within the mudstone itself yielded ratios of 1:120 and 1:111, whereas a measurement within a phosphatic lamina in the same sample resulted in the ratio of 1:1.2 (Fig. 6).

Strontium Isotope Analyses

The evolution in the ratio of $^{87}Sr/^{86}Sr$ isotopes during the Miocene is particularly favorable to precise age dating and a variety of Miocene phosphate deposits have been dated using $^{87}Sr/^{86}Sr$ ratios in phosphates (Compton et al., 1993; Stille et al., 1994; Jacobs et al., 1996). This encouraged us to analyze a series of 17 phosphatic samples (phosphatic peloids, laminae, and crusts) from the vicinity of the condensed interval for their $^{87}Sr/^{86}Sr$ ratios. The measured $^{87}Sr/^{86}Sr$ ratios translate into ages between as old as 17 Ma and ca. 12 Ma, with no discernible trend (Fig. 7; Table 4). Unfortunately, no good correlation was obtained between the nannofossil-derived ages and the youngest strontium-based ages per stratigraphic level (Fig. 7).

The range in age data obtained from the phosphate samples may be explained by the presence of bentonite throughout the condensed intervals, which may have been a source of strontium with low $^{87}Sr/^{86}Sr$ ratios during phosphogenesis. In addition, potential reworking of phosphate material (see below) may also add complexity to the data.

SEDIMENTARY AND EARLY DIAGENETIC STRUCTURES

The sediments analyzed here show a wealth of sedimentary and early diagenetic structures, which are helpful in the interpretation of depositional mechanisms and early diagenetic processes.

Laminations

The sediments of the Monterey Formation are laminated throughout most of the studied section. A distinction is made between primary laminations, which are related to regular differences in the original composition of deposited sediment, and early diagenetic laminations,

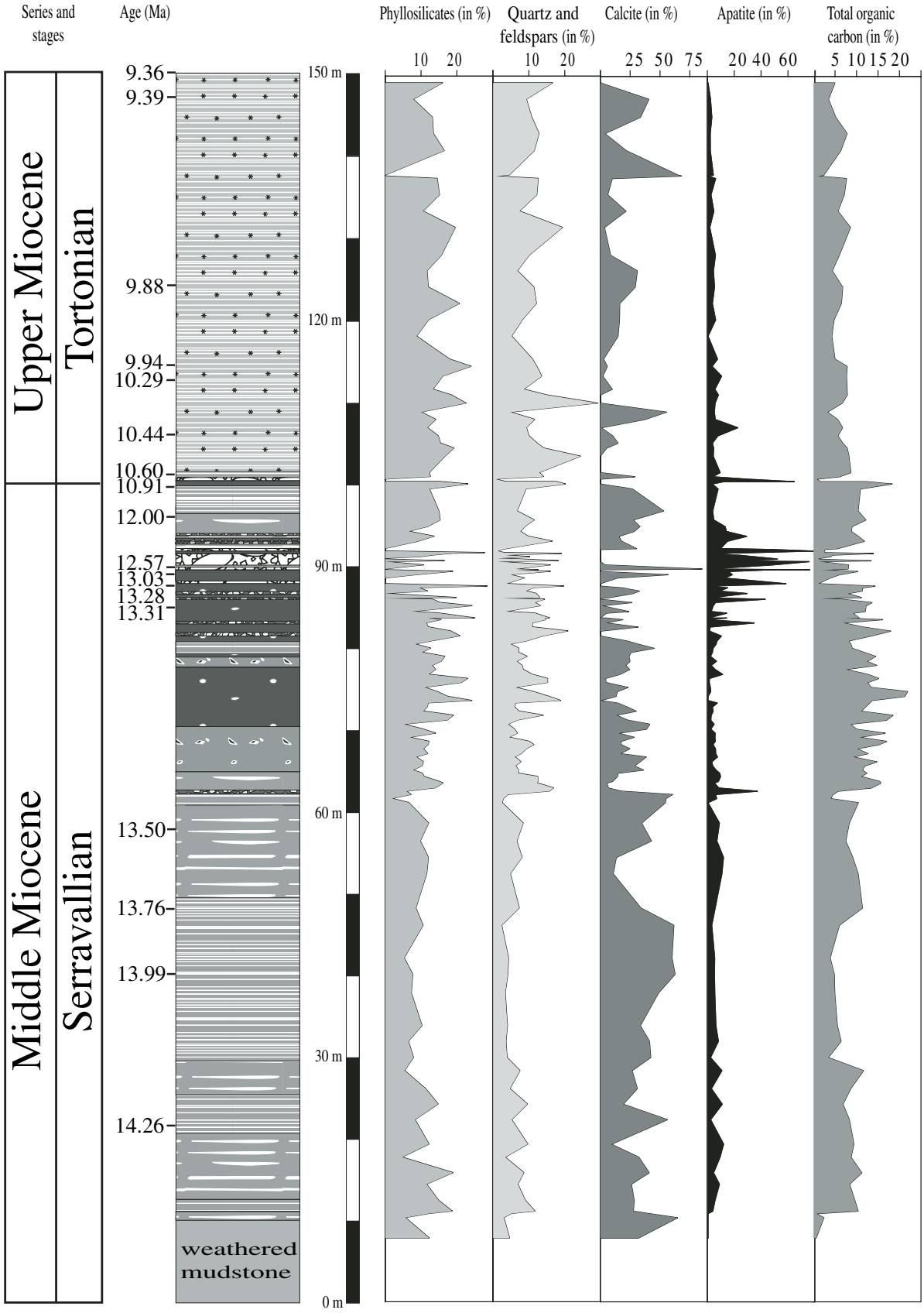

Figure 3. Age dates based on calcareous nannofossils and mineral and total organic carbon distributions obtained for the measured section in the Monterey Formation at Naples Beach. Results obtained from samples in dolomite and bentonite have been omitted.

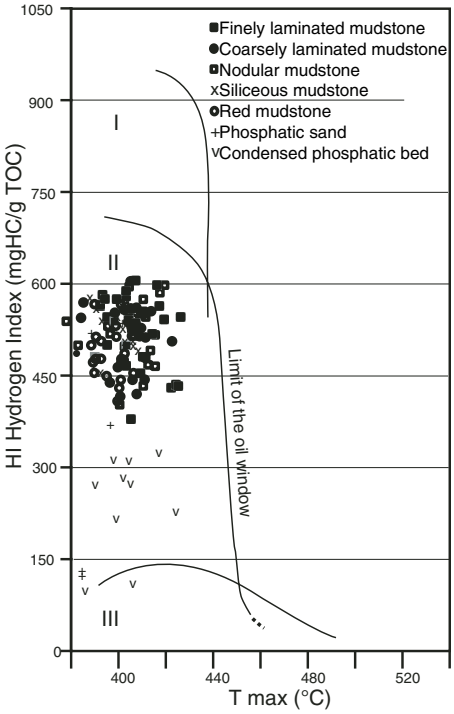

Figure 4. Rock-Eval™6–based analyses of the hydrogen index versus temperature by which a maximum of hydrocarbons are released by thermal cracking (T_{max}) for different lithologies in the Monterey Formation at Naples Beach.

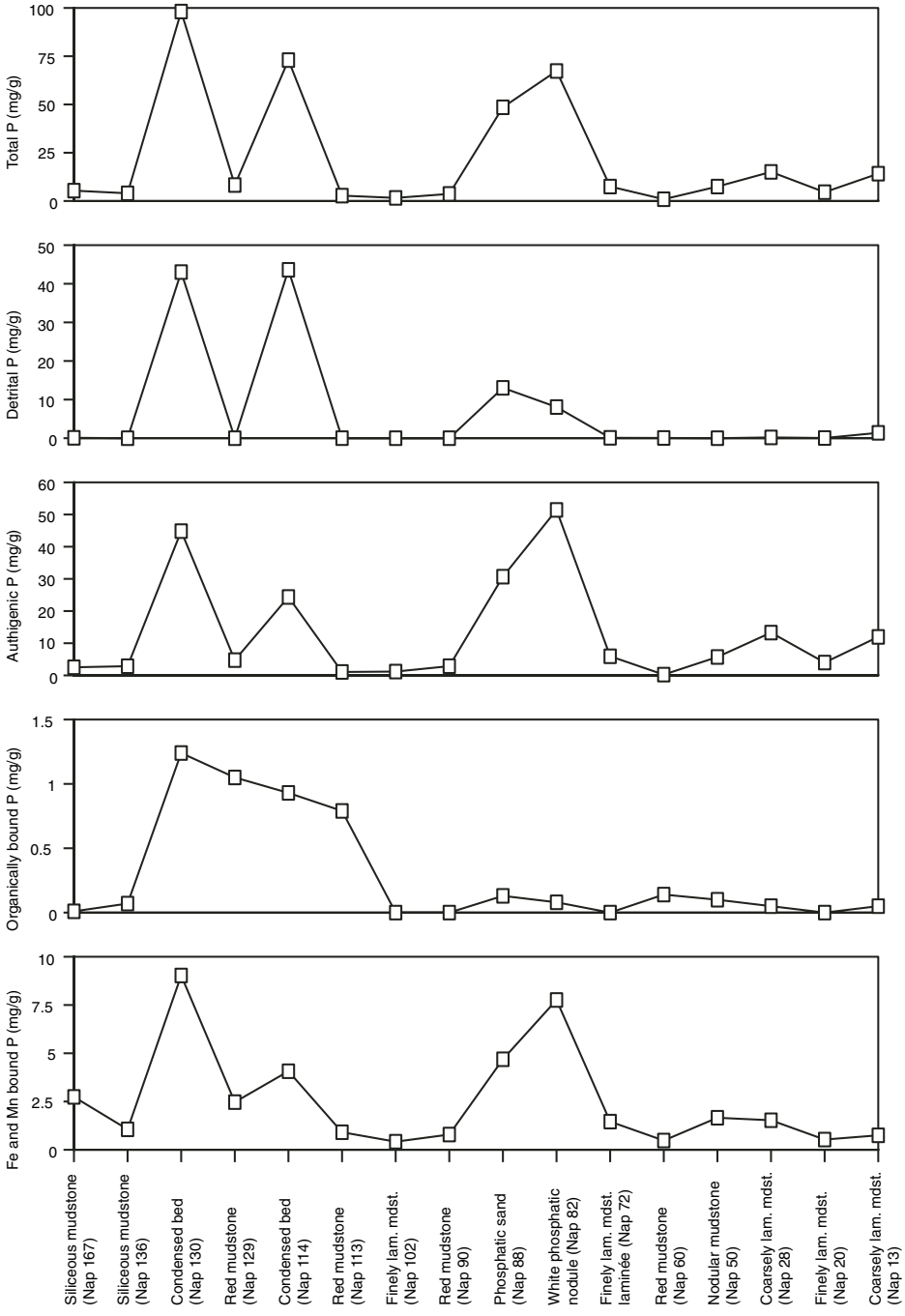

Figure 5. Distribution of different phosphorus phases and total phosphorus contents in a selection of 16 samples of the Monterey Formation at Naples Beach.

which are related to the regular precipitation of phosphate and other minerals in preexisting sediments during early diagenesis. These two types of laminations are end members, and laminations may occur in relation to primary, depositional differences, which are enhanced by early diagenetic precipitations (so-called diagenetically enhanced laminations).

Primary laminations are often nicely preserved in dolomitized intervals in the lower part of the Monterey Formation at Naples Beach; irregular primary laminations occur also in some condensed phosphatic intervals in the middle and uppermost part of the formation (cf. Chang et al., 1998; Johnson and Grimm, 2001). Within the mudstone itself, they are much less conspicuous and early diagenetically formed laminations dominate.

In the dolomitized intervals, the primary laminations consist of dark and organic-rich laminae, light laminae rich in foraminifera, volcanic ash layers, and layers that are internally homogeneous and include isolated flakes of organic matter. These latter layers are comparable to the speckled beds described by Chang and Grimm (1999) from the upper part of the Monterey Formation near Lompoc and interpreted as gravity-flow deposits. The laminations in the dolomitized intervals are often disrupted, contorted (e.g., Seilacher, 1969; Grimm and Orange, 1997), and associated with local discontinuities, slumps, dish structures, and incisive structures (Figs. 8A and 8B).

In a phosphatized bed (which at Naples Beach is only preserved in the form of reworked boulders in the lower part of the overlying Sisquoc Formation), irregularly shaped laminae occur, and they are laterally continuous or discontinuous. The laminated sediments consist of silty phosphatic mudstones. The boundaries between the laminae are covered with a thin layer of silt-free phosphate. These irregular laminations are an example of diagenetically enhanced primary laminations (Föllmi and Garrison, 1991; Föllmi, 1996).

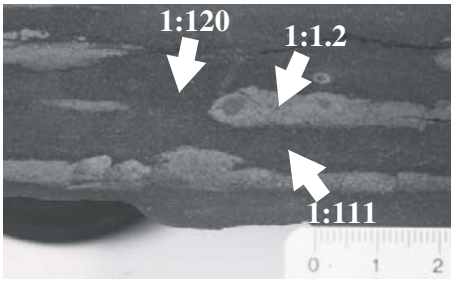

Figure 6. Molar P:C ratios in a representative sample of coarsely laminated mudstone (Nap 23).

Early diagenetically formed laminations dominate the middle part of the Monterey Formation at Naples Beach and structure the sediments in a characteristic way (Figs. 8B and 8C). They are defined by an interplay of dark and organic-rich muddy intervals, ranging in thickness from less than 1 mm to ~2 cm, and light-colored phosphatic laminae, ranging in thickness from less than 1 mm to ~1 cm (so-called pristine phosphate in Föllmi et al., 1991). They are laterally continuous or discontinuous. At their base, the phosphatic laminae usually show a transition to the subjacent muddy intervals, whereas their top is either transitional or defined by a sharp contact. In cases where the top boundary is sharp and well defined, it may show shallow incisive contacts (scours) and lateral cutoffs of the light-colored lamina, leading to a local angular discontinuity (Figs. 8E and 8H). In a few cases, the light laminations show internal deformations, which may lead to an angular discontinuity at its top (Fig. 8F). The presence of angular discontinuities is also observed in the case of whole layer deformation.

In thin section, the phosphate laminae are very irregularly confined, and there are transitions to the organic-rich mudstone, which are characterized by the increasingly dense development of phosphatic microconcretions that coalesce to form the phosphatic laminae. Within the phosphatic laminae, organic-rich mudstone may still be present in the form of thin and irregular seams (Fig. 8G). In cases where the top boundaries of the phosphatic laminae are sharp and well defined, they also appear as such in thin section (Fig. 8H).

Sediment Clasts, Nodules, and Coated Nodules

Sediment clasts are a regularly occurring feature in the Monterey Formation at Naples Beach. They consist either of reworked material from the Monterey Formation itself (e.g., mudstone, dolomite, porcelanite, phosphate) or of exotic material (wood, bone fragments, volcanic material) and are accumulated in discrete horizons or present as isolated clasts. A particularly impressive polymict clastic succession of ~30 m is present immediately west of Dos Pueblo Creek, and a smaller horizon of varying thickness (maximum 1 m) occurs at level Nap 16 (Fig. 2). These successions appear to be part of wholesale slumped intervals.

An isolated dolomite clast marked by *Gastrochaenolites*-type borings was observed in coarsely laminated black mudstone (Fig. 9A). Isolated porcelanite clasts may occur just above porcelanite horizons or elsewhere, unrelated to a porcelanite horizon (Fig. 9B). Isolated clasts of volcanic material, wood fragments, and bone fragments are present in mudstone and within the phosphatic condensed beds; when they occur in mudstone, they may deform and/or interrupt associated phosphatic laminae (Figs. 9C and 9D).

Phosphatic clasts are a widespread phenomenon. They may be isolated or may accumulate in discrete levels composed of sand- to pebble-sized phosphatic lithoclasts (Fig. 9H). The phosphatic clasts may be rounded (Figs. 9E and 9F) or irregularly shaped, light colored or dark colored, and coated by a new phosphate generation (Fig. 9G) or remain uncoated. The coated clasts are usually nodular and may show a sharp and well-defined surface or a transitional boundary to the surrounding mudstone, similar to the early diagenetically formed phosphatic laminae.

Slump-Folded, Perturbed, Fractured, Bioturbated, and Gravity Transported Intervals

Besides entirely slumped intervals, slumps also occur as isolated structures within the mudstone. Phosphatic laminae show single slump folds, which are directly overlain by nondisturbed laminae (Fig. 10A). Mudstone laminae and layers may also show lateral cutoff and

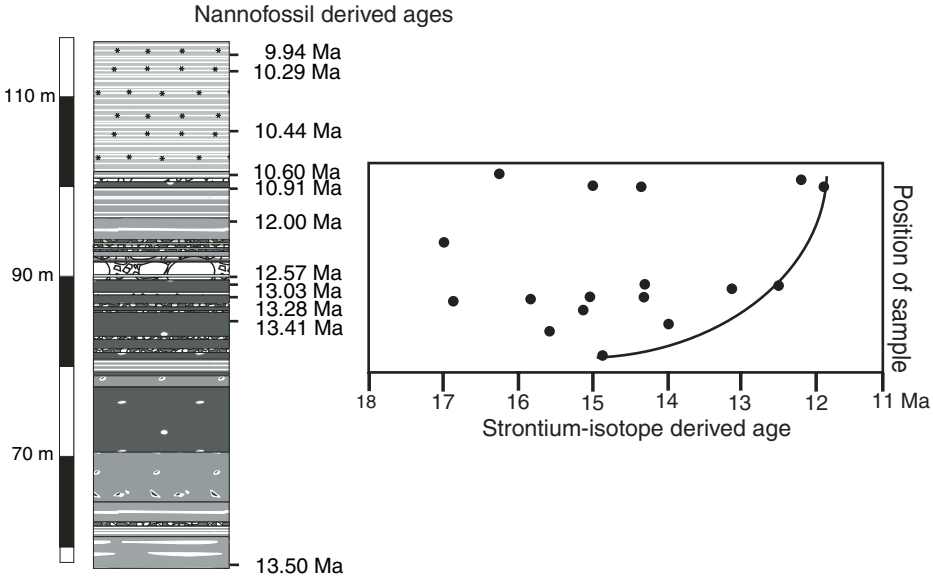

Figure 7. $^{87}Sr/^{86}Sr$ ratios and corresponding apparent ages obtained from a selection of phosphatic samples from the middle part of the Monterey Formation at Naples Beach, compared to nannofossil derived ages.

TABLE 4. VALUES FOR STRONTIUM ISOTOPES IN A SELECTION OF PHOSPHATE SAMPLES FROM THE MONTEREY FORMATION AT NAPLES BEACH

Sample no.	$^{87}Sr/^{86}Sr$	Age
NB5	0.708713(8)	16.25
NB7	0.708809(6)	12.18
NB8A top	0.708758(7)	14.34
NB8A middle	0.708816(6)	11.88
NB8A bottom	0.708743(6)	14.98
NB15	0.708668(7)	16.99
NB18	0.708802(9)	12.48
NB18	0.708759(7)	14.30
NB20	0.708787(6)	13.11
NB24	0.708742(6)	15.02
NB26	0.708759(7)	14.30
NB28	0.708723(6)	15.83
NB29	0.708676(7)	16.86
NB32	0.708740(6)	15.10
NB36	0.708767(7)	13.96
NB37	0.708729(8)	15.57
NB41	0.708746(7)	14.85

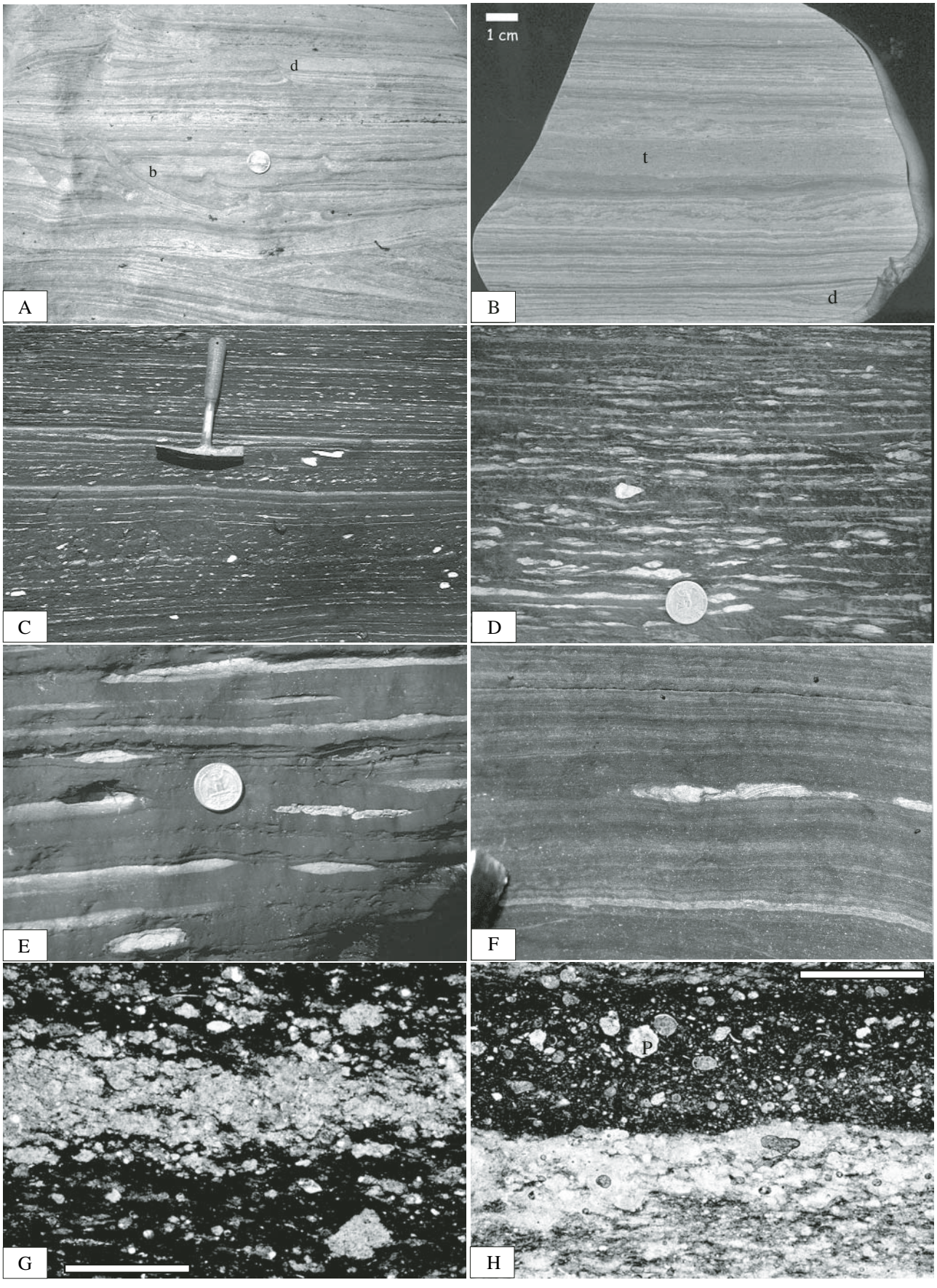
d
b
A
1 cm
t
d
B
C
D
E
F
G
P
H

injection structures (Figs. 10B and 10C; e.g., Dzulynski, 1996). Discrete intervals of up to 50 cm may be perturbed by normal microfaults, or may be amalgamated (Figs. 10D and 10E; Seilacher, 1969; Grimm and Orange, 1997).

Bioturbation is limited to discrete intervals within the Monterey Formation (Föllmi and Grimm, 1990; Ozalas et al., 1994). Unidentified burrows are present in the primary laminated dolomitized intervals (Fig. 8A). *Thalassinoides* burrows occur also in discrete levels within the mudstone succession (e.g., Nap 75; Figs. 10F and 10G). These burrows penetrate the sediments to a depth of up to 20 cm and cut through early diagenetically formed phosphatic laminae in all observed cases.

Gravity-flow deposits occur at all scales. The above discussed conglomeratic intervals are associated with internally slump-folded sediment packages; the amalgamated primary laminations in dolomite beds have been interpreted equally as gravity-flow deposits (Chang and Grimm, 1999). Gravity-flow deposits are also widespread within the mudstone. Internally homogeneous layers up to 20 cm thick, which are sharply bound toward the base and top, are interpreted here as mudflow deposits (Fig. 10H). Gravity-flow deposition may also have been instrumental in the deposition of the black, organic-rich muddy laminae, as is shown below.

Structures in Condensed and Allochthonous Phosphatic Beds

The condensed phosphatic beds in the Monterey Formation at Naples Beach are characterized by a variety of stratification types, which differ in complexity and appear to be based on some sort of interplay between phosphogenesis, episodes of nondeposition and erosion, and gravity-flow deposition (Figs. 11–13; Garrison et al., 1987, 1990, 1994; Föllmi et Garrison, 1991; Föllmi et al., 1991; John et al., 2002). Three end members are observed. (1) Condensed phosphatic beds consisting of stacked and/or coalesced phosphatic laminae, with reduced (stacked) or without (coalesced) intervening mud laminae (Figs. 11A, 11C, 11D, and 12B). (2) Conglomeratic condensed phosphatic beds, which include phosphatic clasts and grains. These clasts result from the fragmentation of one or more phosphatic laminae and the consequent concentration by winnowing (Fig. 11B). (3) Allochthonous phosphatic beds, which are composed of polymict conglomeratic layers and result from the erosion of preexistent phosphatic beds and their redeposition by gravity flow (Fig. 12D).

Complexity is added by the following. (1) In the condensed beds consisting of stacked or coalesced phosphatic laminae, intervening erosive boundaries and related angular unconformities may be present (Figs. 11C and 12E). (2) The winnowed and allochthonous conglomeratic layers may become cemented by subsequent phases of phosphogenesis (Figs. 11D, 11E, 11F, 12A, 12C, and 12D). (3) The conglomeratic layers may include detrital quartz grains, wood and bone fragments, and volcanic pebbles (Fig. 12D) and/or layers and particles of different authigenic minerals, such as glauconite (Fig. 12C), dolomite (Fig. 11D; Garrison et al., 1994), and silica phases.

In thin section, the internal architecture of the condensed and allochthonous phosphatic beds reveals itself as complex (Fig. 13). The stacked and often coalesced phosphatic laminae include large amounts of phosphatic particles, such as phosphatized benthic calcareous or agglutinated foraminifera (Figs. 13A and 13B), phosphatized coprolites and peloids (Figs. 13B, 13C, and 13H), fish debris (Figs. 13E–13G), phosphatized lithoclasts, and glauconite grains (Fig. 13I). The phosphatic particles are often complex, marked by different phases of phosphogenesis and signs of sediment reworking and re-exposure (Figs. 13J–13O). This is shown by (1) nodules, which consist of different phosphatic generations characterized by different color and facies (Figs. 13C, 13K–13M); (2) coated grains, which consist of phosphatic particles enveloped by a separate phosphate phase (Fig. 13D); (3) coalesced particles (Fig. 13L); and (4) phosphatic particles that are peripherically bored, encrusted, and eroded (Fig. 13J). Fragmented phosphatic laminae may serve as a source of phosphatic lithoclasts and particles (Fig. 13O), which may consequently be incorporated into winnowed and/or allochthonous layers.

Structures and Phosphate Mineralogy: ESEM/EDS Analyses

We used an environmental scanning electron microscope (ESEM) coupled to an energy dispersive spectrometer (EDS) in order to elucidate the microstructure and mineralogy of a selection of representative phosphates, including (1) a light-colored phosphatic lamina (Nap 13 in Fig. 2); (2) a light-colored phosphatic nodule (Nap 80 in Fig. 2); and (3) a condensed phosphatic horizon (Nap 89 in Fig. 2; cf. Fig. 11E). The phosphate mineral is carbonate fluor-apatite in all three samples.

The microstructures are distinctive and appear to be dependent on the type of phosphate (Fig. 14). The phosphate in the phosphatic lamina (Nap 13) is composed of 1–2 μm long, rod-like structures, which appear isolated, in crossed twins, or in bundles (Figs. 14A–14C). Locally, they are linked by isolated filamentous structures (Fig. 14C). Similar structures

Figure 8. Close-up photographs and photomicrographs (scale bar = 1 mm in all images; nonpolarized transmitted light) of primary and early diagenetically formed laminations in the Monterey Formation at Naples Beach. (A) Primary laminations in a dolomitized interval showing laterally discontinuous laminae, angular unconformities, localized water-escape structures (d), and burrows (b); (B) primary laminations in a dolomitized interval with finely laminated intervals near the bottom and top of the sample, which consist of light-colored, calcareous laminae and dark-colored, organic-rich laminae, whereas the coarse layer in the middle of the sample consists of a mixture of calcareous material and particles and flakes of organic matter (t). The finely laminated interval in the lower part of the sample shows a discordance on its right side (d); (C) early diagenetically formed phosphatic laminae showing thicker, laterally continuous and thinner, laterally discontinuous laminae in red mudstone. Several intervals underneath hammer are perturbed by synsedimentary fracturing (Nap 84). The dark mudstone includes light-colored phosphatic clasts and nodules; (D) laterally discontinuous early diagenetically formed phosphatic laminae and lenses in coarsely laminated black mudstone that contains an isolated phosphatic clast (near Nap 28); (E) laterally continuous and discontinuous early diagenetically formed phosphatic laminae in coarsely laminated black mudstone showing transitional bases, sharp upper limits, and local shallow incisive structures. Exact location within section not determined; (F) laterally discontinuous phosphatic lamina in siliceous mudstone, which is contorted. The contact with the overlying dark lamina is well defined and erosive. Exact location within section not determined; (G) photomicrograph of laterally discontinuous early diagenetically formed phosphatic lamina in coarsely laminated black mudstone; the lamina consists of coalesced phosphatic microconcretions, which are also present in the muddy matrix in a more dispersed form (Nap 7); (H) photomicrograph of a sharply bound and well-defined top contact of an early diagenetically formed phosphatic lamina. Overlying mudstone contains phosphatic particles (P) (Nap 7).

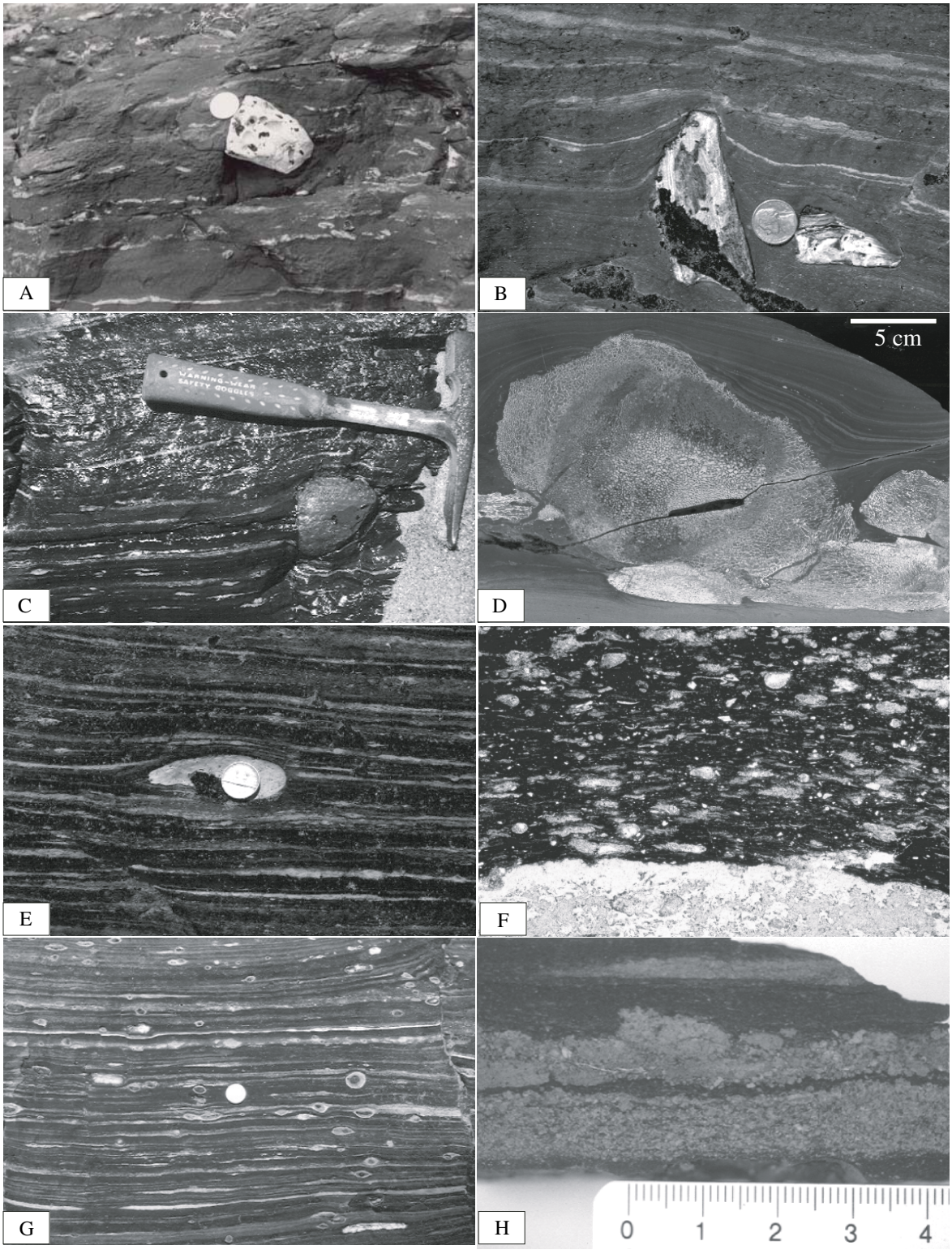

Figure 9. Lithoclasts in the Monterey Formation at Naples Beach. (A) Isolated, surficially bioeroded dolomite clast in coarsely laminated black mudstone. Exact location within section not determined; (B) two isolated chert clasts in siliceous mudstone. Exact location within section not determined; (C) exotic nodule of volcanic material in coarsely laminated black mudstone. Exact location within section not determined; (D) cetacean bone fragments in siliceous mudstone. Sample by courtesy of Richard Behl (California State University, Long Beach); (E) Phosphatic nodule in finely laminated black mudstone. Exact location within section not determined; (F) photomicrograph of the sharp and well-defined margin of a phosphatic nodule in nodular black mudstone (Nap 42); (G) coated phosphatic nodules in nodular black mudstone. Exact location within section not determined; (H) slabbed sample of a sandy phosphatic lamina in siliceous mudstone (Nap 118).

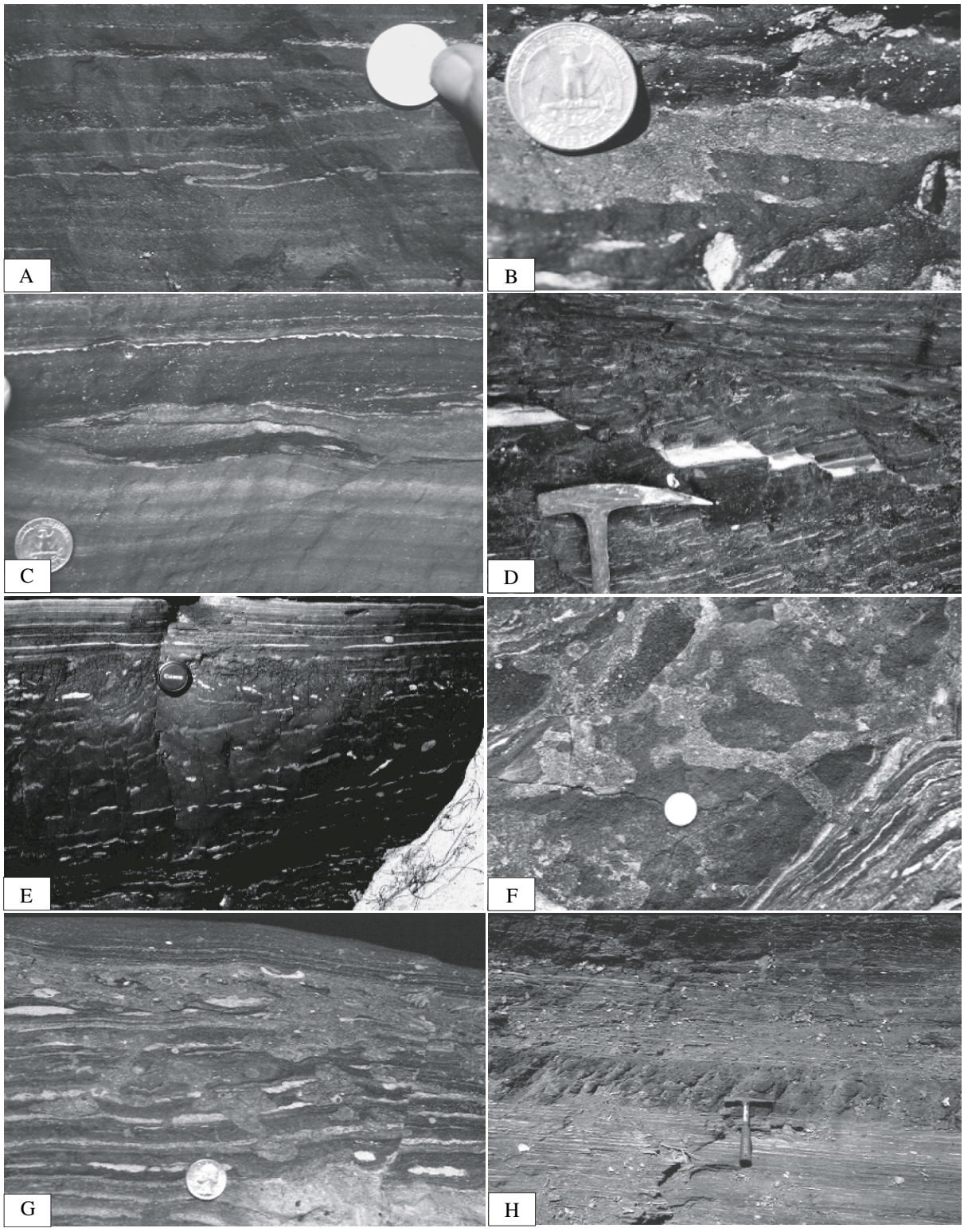

Figure 10. Fractured, perturbed, slump-folded, bioturbated, and gravity-flow intervals in mudstone of the Monterey Formation at Naples Beach. (A) Slump-folded phosphatic lamina in mudstone at 62.8 m in Figure 2; (B) a layer of red mudstone is laterally cut off by a sandy phosphatic layer, which partly lifts up the remaining mudstone layer (Nap 66); (C) finely laminated dark mudstone partly undercutting the subjacent, lighter-colored mudstone layer (Nap 34); (D) bentonite layer fractured by a series of normal, unidirectional, synsedimentary microfaults (Dat 21); (E) perturbed interval in coarsely laminated siliceous mudstone (Nap 149); (F–G) interval marked by *Thalassinoides* burrows cutting through early diagenetically formed phosphatic laminae; burrows are infilled with phosphatic sand (Nap 75); (H) internally homogeneous mud-flow deposit within coarsely laminated black mudstone.

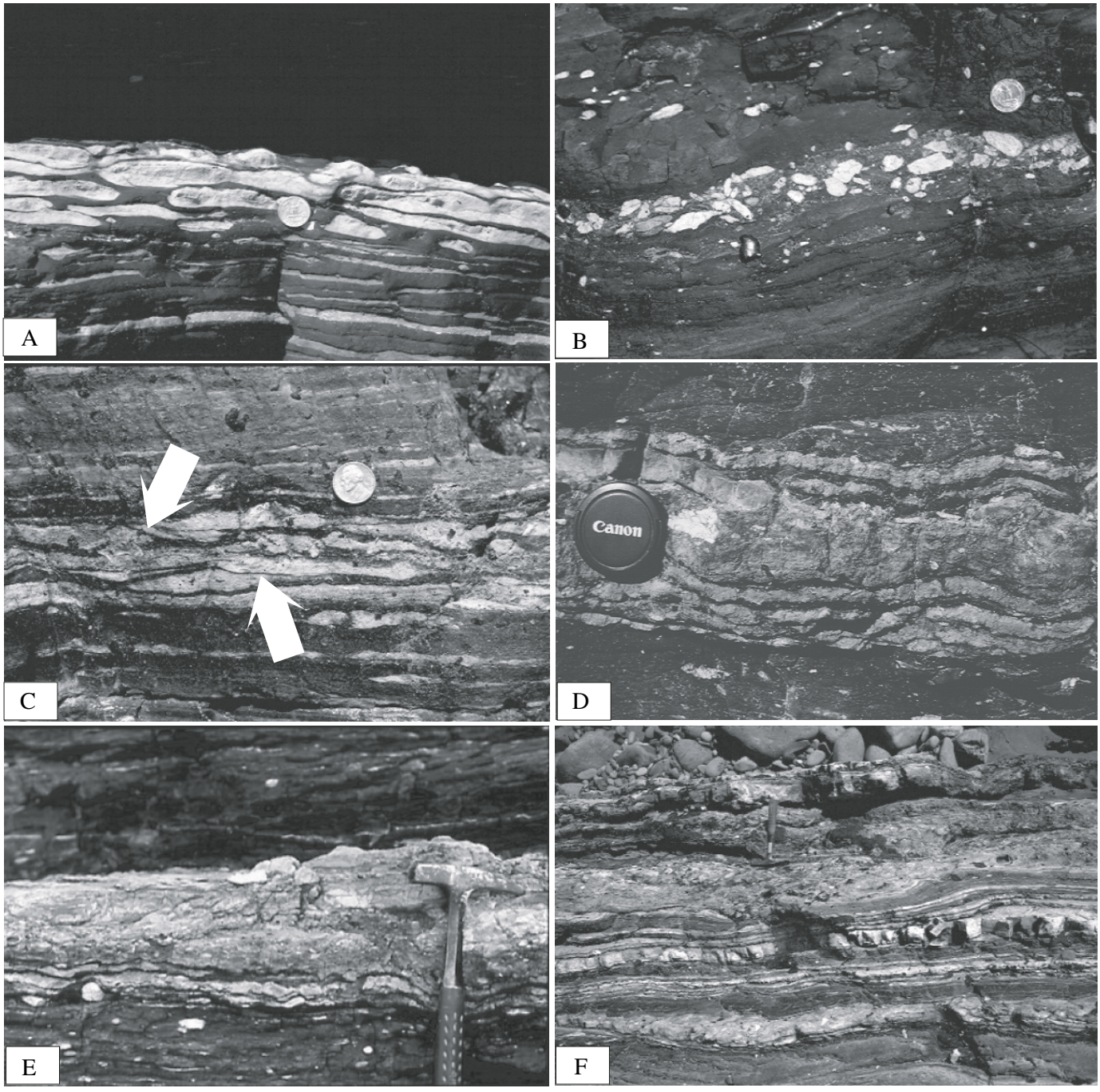

Figure 11. Condensed phosphatic horizons in the Monterey Formation at Naples Beach. (A) Interval in coarsely laminated black mudstone in which phosphatic laminae and lenses are closely spaced (stacked) (Nap 37); (B) discrete conglomeratic level consisting of phosphatic nodules and clasts in red mudstone (Nap 82); (C) stacking of coarse phosphatic laminae and lenses in coarsely laminated black mudstone. Some laminae are cut off laterally and separated from the next generation of phosphatic lenses by an angular unconformity (arrows). Exact location in the section not determined; (D) condensed phosphatic interval composed of stacked phosphatic laminae and lenses at the base, a conglomeratic layer with a partly phosphatized matrix (cf. Fig. 12A) in the middle, and stacked phosphatic laminae and lenses at the top. A laterally discontinuous dolomite layer is visible just above the lens cap (Nap 95); (E) condensed phosphatic interval composed of an entirely phosphatized conglomeratic phosphatic bed with a level of stacked phosphatic laminae at its base (Nap 88 and 89); (F) a series of condensed phosphatic intervals, which consists of entirely phosphatized conglomeratic layers, coalescent phosphatic laminae, and closely spaced phosphatic laminae (Nap 105–109).

have been described from the same locality by Reimers et al. (1990), and comparable, albeit somewhat larger structures have been reported from recent phosphorites offshore of Peru (ODP Leg 112; Lamboy, 1994; compare also Mirtov et al., 1987). The light-colored phosphatic nodule shows an internal structure composed of phosphatic microspheres, which are 2–10 µm in size (Fig. 14D). Such structures are also documented from recent phosphorites offshore of Peru (Lamboy, 1994) and elsewhere (Soudry and Lewy, 1988; Mirtov et al., 1987). This sample includes also phosphatic molds of diatom tests (Fig. 14E). The condensed phosphatic horizon (Nap 89) is composed of phosphates, which are better crystallized and include idiomorphic crystals (Figs. 14F–14H). Pore spaces are lined with botryoidal, radiating phosphatic envelopes, which include idiomorphic, hexagonal, phosphate crystals of 2–5 µm (Fig. 14F). Similar structures are also shown in Mirtov et al. (1987).

INTERPRETATIONS

General Trends in Sediment Accumulation

The combination of XRD, TOC, and phosphorus analyses on a large selection of representative samples and biostratigraphic time control allows us to quantify accumulation rates of total sediment, TOC, phosphorus, and a selection of other minerals (in mg/cm^2/k.y.; Fig. 15). In our calculations, we used a dry bulk density value of 1.35 g/cm^3 for mudstone. This is the average value obtained by measuring five typical mudstone samples (Nap 33, finely laminated black mudstone: 1.6 g/cm^3; Nap 50, nodular black mudstone: 1.42 g/cm^3; Nap 69, nodular black mudstone: 1.22 g/cm^3; Nap 74, red mudstone: 1.22 g/cm^3; Nap 157, siliceous black mudstone: 1.32 g/cm^3).

1. The time interval between ca. 14.3 and 13.5 Ma is characterized by the deposition of mainly finely and coarsely laminated black mudstone. The average nondecompacted sedimentation rate is ~49 m.y. and the average sediment accumulation rate corresponds to 6620 mg/cm^2/k.y. The average TOC value is 8.54 wt% and the average TOC accumulation rate is 565 mg/cm^2/k.y. Average phosphorus contents amount to 0.89 wt%, which gives an average phosphorus accumulation rate of ~60 mg/cm^2/k.y. Calcite contents average to 35 wt% due to the abundance of benthic foraminifera and nannoplankton, and accumulation rates correspond to 2320 mg/cm^2/k.y.

2. The time interval between 13.5 and 13 Ma saw a change from laminated black mudstone to nodular black and red mudstone. Sedimentation and sediment accumulation rates correspond to ~66.2 m/m.y. and 8935 mg/cm^2/k.y., respectively. Average TOC values amount to 12.66 wt%; the corresponding TOC accumulation rate is 1130 mg/cm^2/k.y. Phosphorus contents average to 0.764 wt% and the phosphorus accumulation rate averages to 70 mg/cm^2/k.y. Calcite contents progressively and irregularly diminish toward the top of this interval (see also Fig. 5), which is due to a change from calcitic toward agglutinated foraminifera, and the average calcite content is 22 wt%. The calcite accumulation rate is 1980 mg/cm^2/k.y.

3. The time interval between 13 and 10.6 Ma is characterized by a change from red mudstone toward coarsely laminated black and siliceous mudstone and by the presence of condensed phosphatic horizons. Sedimentation and sediment accumulation rates are correspondingly low and amount to 4.8 m/m.y. and 645 mg/cm^2/k.y., respectively. An average value of TOC for this interval is 8.58 wt%, and the corresponding accumulation rate is 55 mg/cm^2/k.y. The average phosphorus content is 1.75 wt%, and its accumulation rate is 10 mg/cm^2/k.y. Calcite contents amount to 21 wt% and the accumulation rate corresponds to 135 mg/cm^2/k.y.

4. In the time interval between 10.6 and 9.4 Ma, sedimentation is dominated by siliceous mudstone. Sedimentation and sediment accumulation rates correspond to values of 39.6 m/m.y. and 5345 mg/cm^2/k.y., respectively. Average TOC contents amount to 6.03 wt% and TOC accumulation rates equal 320 mg/cm^2/k.y. Phosphorus contents are around 0.5 wt%, and phosphorus accumulation rates are calculated as 25 mg/cm^2/k.y. Average calcite contents approximate 16.88 wt%, which corresponds to an accumulation rate of 900 mg/cm^2/k.y.

Calculated organic carbon accumulation rates vary between 55 and 1130 mg/cm^2/k.y., whereby the highest measured TOC values correspond to the period of high TOC accumulation (cf. Isaacs, 2001). An average value of 310 mg/cm^2/k.y. is obtained for the entire investigated time interval. An overall lower but similarly variable trend in TOC accumulation was observed in the section at El Capitan State Beach (John et al., 2002), with values between 190 and 390 mg/cm^2/k.y. for the period between 16.48 and 13.3 Ma, 0–30 mg/cm^2/k.y. for the period between 13.3 and 10.8 Ma, and 90 mg/cm^2/k.y. from 10.8 Ma onward. The average value is 150 mg/cm^2/k.y.

TOC and phosphorus accumulation patterns are comparable, with the highest accumulation rates occurring in the time interval of 13.5 and 13 Ma. The time interval with the highest quantities of phosphorus (between 13 and 10.6 Ma) corresponds to the lowest accumulation rate. The highest accumulation rates for calcite are observed between 14.3 and 13.5 Ma. Quartz, feldspar, and phyllosilicate accumulation rates are highest for the period from 13.5 to 13 Ma (Fig. 15).

Sediment Accumulation Processes

Sediment deposition and accumulation in the Monterey Formation appear to have been governed for a large part by episodic and highly dynamic processes. Indications for this are manifold.

1. Sediments with preserved primary laminations show the presence of disrupted and contorted beds, local discontinuities, slumps, water-escape structures, and erosive structures (Fig. 8).

2. Internally homogeneous laminae and layers, including isolated flakes of organic matter, have been interpreted as gravity-flow deposits (Fig. 8B; Chang and Grimm, 1999).

3. Slumping is observed on the scale of entire sediment units, but also in thin intervals, for example in phosphatic laminae (Fig. 10A).

4. Mud-flow deposits occur in the form of internally homogeneous mud beds (Fig. 10H).

5. Phosphatic laminae show incisive structures at their top, which may laterally cut off the laminae (Fig. 8E). Contorted laminae (Fig. 8F), angular discontinuities interfacing the laminae (Fig. 8E), and injection structures (Figs. 10B and 10C) are additional indicators of dynamic conditions.

6. The presence of clasts, nodules, coated phosphatic nodules, and phosphatic grains within the muddy intervals is viewed here as the result of erosion and subsequent transport by gravity flow (Fig. 9).

7. The presence of condensed and allochthonous phosphatic beds and their complex internal architecture (Figs. 11–13) are taken here as indicators of important hydrodynamic conditions.

8. The presence of *Thalassinoides* in isolated horizons within the laminated sediments (Figs. 10F and 10G)—not associated with other types of bioturbation—is an indication of crustacea, which survived turbulent gravity-flow transport and subsequent dysaerobic conditions (doomed pioneers; Föllmi and Grimm, 1990; Grimm and Föllmi, 1994).

The sum of these observations suggests that gravity-flow deposition was an important process in the deposition of the mudstone. A non-negligible part of the mudstone was deposited episodically in the form of distal turbidity currents and subordinated mud flows, thereby locally eroding and/or perturbing the subjacent sediment cover (cf. Stow et al., 2001).

The formation of fractured and perturbed sediment intervals in the Monterey Formation has been related previously to seismic activity (Seilacher, 1969; Grimm and Orange, 1997). We tentatively extend this mechanism to the

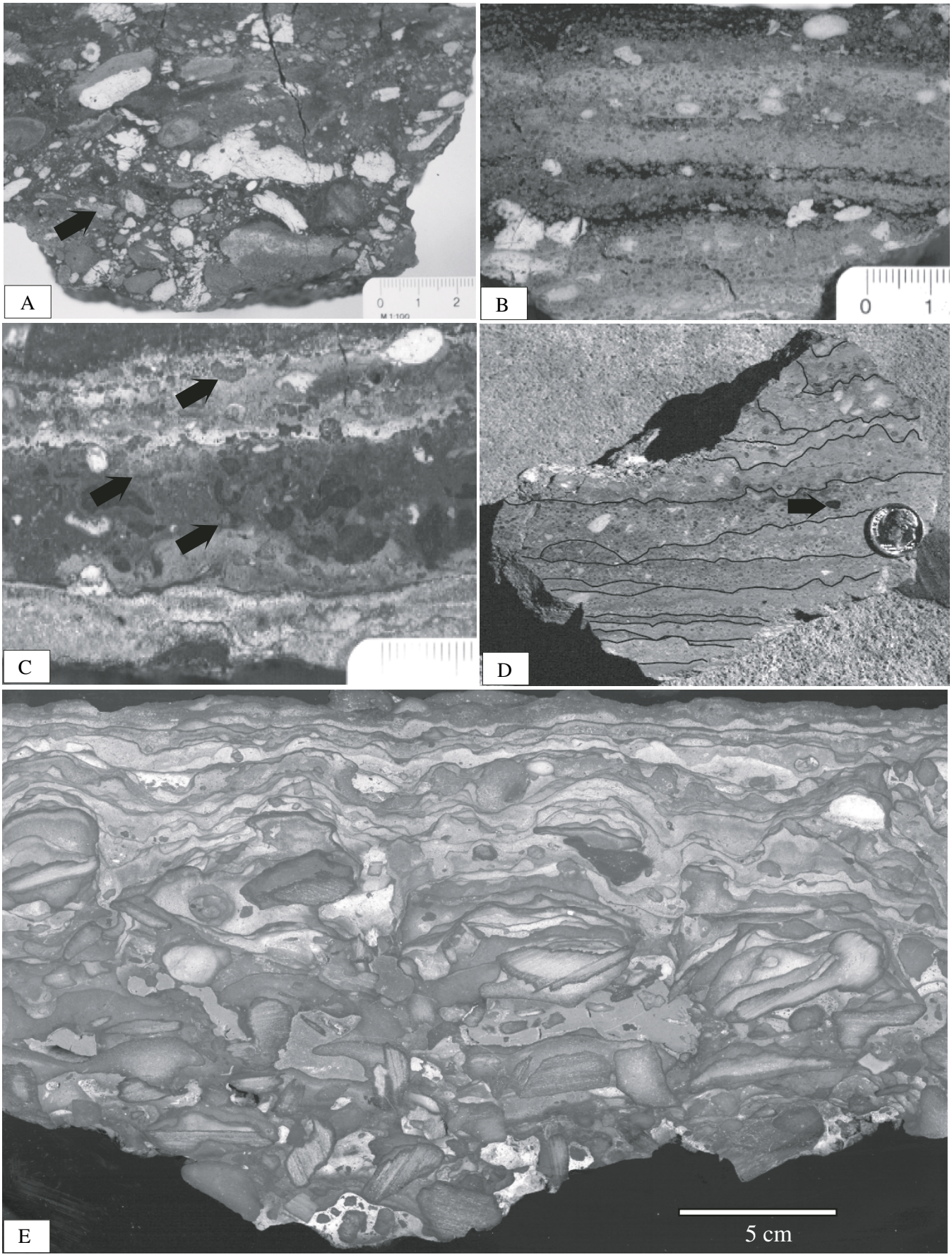
A
B
C
D
E
5 cm

processes ascribed above and propose that seismic activity was instrumental in shaping the sediments of the Monterey Formation, by the in situ deformation of sediments, thereby facilitating the erosion and reworking of preexisting sediments and episodically triggering slides and gravity flows.

Bottom-current activity has been instrumental as well in lowering sediment accumulation rates, inducing episodes of nondeposition, winnowing, and erosion. It may also have been important in accelerating the transfer of inorganic phosphate from bottom water into the sediment (see below). In general, the intensity of these processes—gravity-flow deposition, seismic activity, and bottom current activity—reached a maximum in the period between 13 and 10.6 Ma, where condensation of sediments prevailed and accumulation rates dropped to a minimum.

Early Diagenesis and the Formation of Phosphatic Laminae

The mineralogical composition of the Monterey Formation at Naples Beach is influenced by early diagenetic processes, which lead to the precipitation of dolomite, porcelanite and chert, and especially phosphate. We focus here on the precipitation of phosphatic laminae and suggest that they were formed at a very early stage of diagenesis. Evidence for this is that the phosphatic laminae have frequently been subjected to subsequent shallow scouring and erosion (Fig. 8E) and that they are involved in subsequent phases of sediment deformation such as slumping, fracturing, and bioturbation (Figs. 10A, 10D–10G). They do not appear to have formed directly at the sea floor but may have formed just below this interface. This is suggested by the examination of noneroded phosphatic laminae in thin section, which show transitional zones toward the overlying mudstone (Fig. 8G).

Early diagenetic dolomitization occurred regularly and may preserve precompacted sedimentary structures (Figs. 8A and 8B). The thus-formed dolomite may be subsequently eroded and reworked as nodules thereby undergoing biological erosion (Fig. 9A). Reworked dolomite nodules appear in wholesale slumped intervals; they are, however, not observed in thin allochthonous beds, which suggests that their formation occurred deeper below the sediment-water interface (probably several meters), only to be reworked during large-scale erosional events. This is compatible with observations of Burns and Baker (1987), who, based on geochemical and stable carbon isotopic evidence, postulated a formation depth of not more than several meters. Similar observations are made for reworked porcelanite nodules, which may appear less than a meter above porcelanite horizons (Fig. 9B). In analogy, their reworking appears to be restricted to large-scale erosional events, and their formation depth may equally correspond to several meters (cf. Behl, 1992; Behl and Garrison, 1994).

Accumulation and Preservation of Organic- and Phosphate-Rich Sediments

The challenge here is to develop a model of organic matter and phosphate accumulation, which is compatible with the reconstructed dynamics and resulting moderate organic carbon accumulation rates (Table 5). The average organic carbon accumulation rate for the Monterey Formation at Naples Beach corresponds to ~8% of the average rate for the high productivity region offshore of Peru during the Holocene (3700 mg/cm^2/k.y.; 6 different sites, Table 5; Reimers and Suess, 1983; Tamburini, 2001; Isaacs, 2001; John et al., 2002). The rate is comparable to average values of coastal nonupwelling sites (70–300 mg/cm^2/k.y.; Stein, 1991) or to deeper basins with moderate preservation rates (Table 5). The moderate values for Naples Beach are mainly due to the episodic character of depositional processes and intervening episodes of nondeposition, winnowing, and erosion. The accumulation rates calculated for Naples Beach are not related to the quantity of organic matter directly received from primary production by accumulation from suspension but rather to the balance between the quantity of organic matter received by gravity-flow deposition from shallower areas and the quantity of organic matter lost by winnowing, erosion, and removal to deeper areas. This implies that the generally high TOC values of up to 22 wt% are the product of excellent preservation conditions, which overruled the negative effects on organic matter preservation resulting from sediment accumulation dynamics (e.g., Müller and Suess, 1979; Stein, 1991; Wignall, 1994). This was previously observed by Isaacs (2001) and Piper and Isaacs (2001), who noted a relationship between low sediment accumulation rates and high organic matter preservation rates, which is not necessarily related to high productivity rates and accompanied by high dissolution rates of calcite and silica.

The process of phosphogenesis and formation of phosphatic laminae may have been helpful in improving the conditions of organic matter preservation. These laminae were formed close to the sediment-water interface, very shortly after deposition of the organic-rich mud. By precipitating phosphate in the pores of the organic-rich mud, laminae stabilized the surface sediment at an early stage of diagenesis, rendered the sediment less permeable (Figs. 14A–14C), and served as a sediment lid, thereby protecting the subjacent muddy sediment and preserving the organic matter enclosed there (see also John et al., 2002). This is certainly not the only process involved in the enhanced preservation of organic matter. Even if the phosphatic laminae are a common feature in the Monterey Formation at Naples Beach, they are not ubiquitous and are rather rare in red mudstone, the mudstone with the highest TOC values. Free oxygen contents in the bottom water were probably lowest during deposition of the red mudstone,

Figure 12. Slabbed samples of condensed phosphatic horizons in the Monterey Formation at Naples Beach. (A) Conglomeratic phosphatic level that consists of different types of phosphatic pebbles and particles embedded in a muddy, partly phosphatized matrix. Some volcanic particles occur as well (arrow) (Nap 95; cf. Fig. 11D); (B) condensed phosphatic horizon consisting of stacked, partly coalesced phosphatic laminae, with locally preserved muddy intervals (Nap 106; cf. Fig. 13A); (C) condensed phosphatic bed consisting of phosphatized layers and laminae, which are partly conglomeratic and include glauconite (arrows) (Nap 130); (D) condensed phosphatic bed composed of thin and irregular phosphatic laminae, which include phosphatized particles and rarely also volcanic lithoclasts (arrow). The boundaries between the laminae are marked by erosion and particle reworking at the base. Note that the laminae becomes thicker and more irregular toward the top and that the included phosphatic lithoclasts increase in size as well (NB 26; compare also Figure 7 *in* Föllmi et al., 1991); (E) condensed phosphatic bed from the uppermost part of the Monterey Formation reworked as large clasts in basal sediments of the overlying Sisquoc Formation. This bed consists of a succession of irregularly shaped phosphatic laminations, which are laterally continuous or discontinuous, and partly envelop cm-sized clasts of reworked porcelanites. The laminated sediments are phosphatized and the degree of phosphatization increases toward the top of each lamination. These irregular laminations are an example of diagenetically enhanced primary laminations (cf. Figure 13N; Föllmi et al., 1991; Föllmi and Garrison, 1991; Föllmi, 1996).

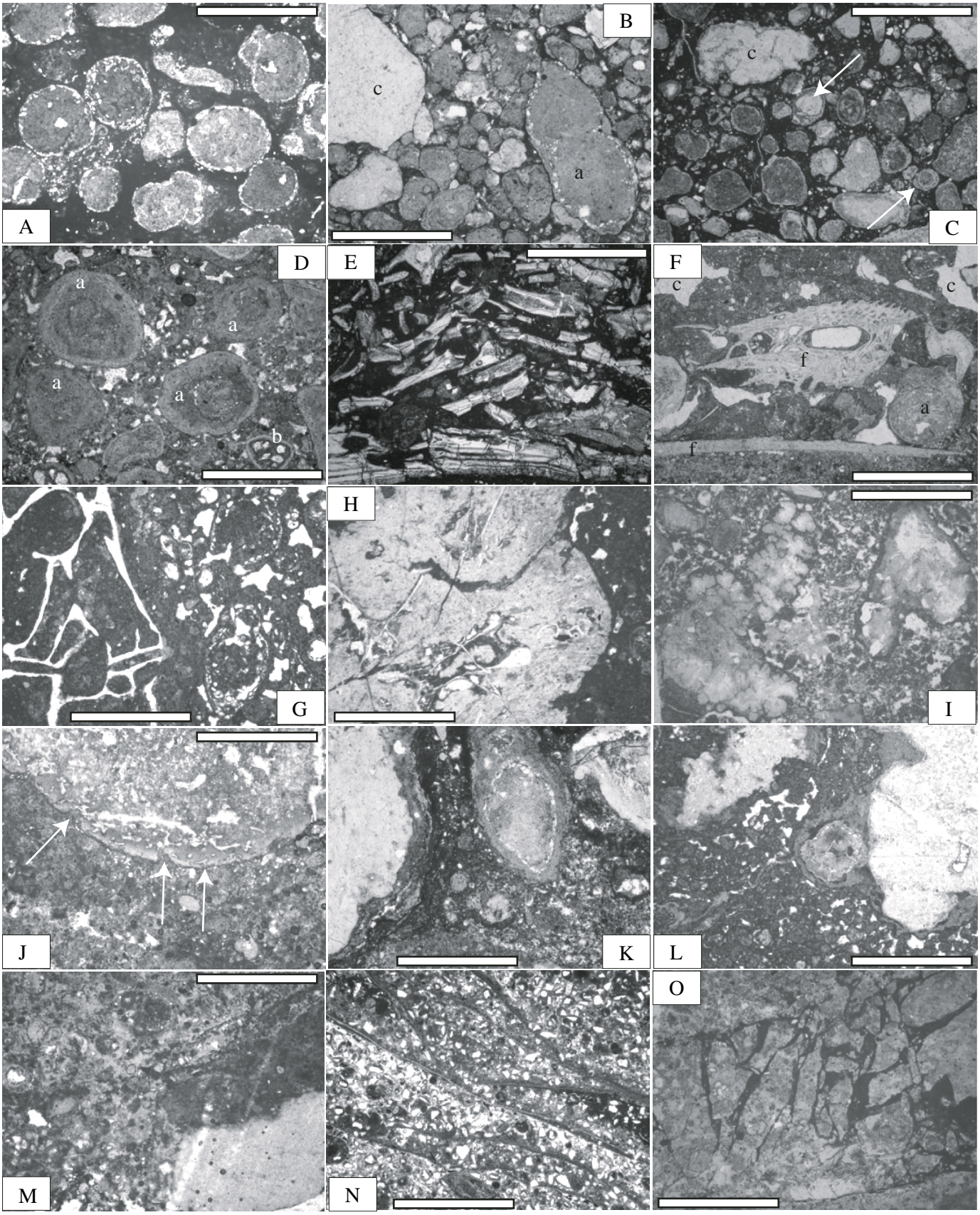
A
B
c
a
C
c
D
a
a
a
a
b
E
F
c
c
f
a
f
G
H
I
J
K
L
M
N
O

as is indicated by the disappearance of calcareous benthic foraminifera and the prevalence of agglutinated foraminifera (Isaacs, 2001; John et al., 2002), and this may have helped as well in the preservation of organic matter (Stein, 1991; Wignall, 1994).

The relationship between phosphogenesis and organic matter preservation is examined here also with regard to the P:C molar ratio in selected whole-rock samples. Deviations of this ratio from the Redfield ratio imply that either the organic matter was degraded and a relative loss of phosphorus occurred (which may have been used for phosphogenetic processes or transferred back into the ocean at a ratio higher than Redfield ratio), or that the sediments became enriched in phosphorus from an external source or became impoverished in organic carbon, relative to organic phosphorus (ratio lower than Redfield ratio). The molar P:C ratios of 1:120 and 1:111 measured on a representative coarsely laminated mudstone sample (excluding phosphatic laminae; Nap 23; Fig. 6) are very similar to the Redfield ratio. This suggests that for this sample, the organic-rich mud has preserved its original P:C molar ratio, thereby precluding a major transfer of phosphorus derived from the degradation of organic matter to the phosphatic laminae.

If phosphogenesis would have been driven entirely by the degradation of organic matter and transfer of organic phosphorus into phosphates, and the sedimentary system would have remained closed for externally derived phosphorus, one would expect P:C ratios to be similar to the Redfield ratio in whole rock samples. The P:C molar ratio averaged for five whole rock samples (including phosphatic laminae), however, is 1:55, which suggests general enrichment of the sediment in phosphorus relative to organic carbon. Earlier calculations have shown that theoretically a 2-cm-thick mud layer with 10% TOC would only produce an ~0.5-mm-thick layer of pure apatite, if a complete transfer of phosphorus from the degradation of organic matter, dissolution of fish debris, and reduction of Mn and Fe compounds is assumed (Föllmi and Garrison, 1991). The thus-obtained theoretical ratio of 2 cm mud and 0.5 mm phosphate (=40:1) does not correspond to the observed ratio of ~5–10:1 (compare Figs. 8C and 8D).

These observations suggest that the phosphorus used in the process of phosphogenesis was derived from an external source thereby enriching the sediments in phosphorus, rather than from an internal source such as the decomposition of buried organic matter and fish debris and desorption of phosphorus from Fe and Mn compounds upon reduction. This is also compatible with the observation that in several cases, phosphate concentrations appear to increase toward the top of the phosphatic laminae (e.g., Fig. 12E), which is suggestive of a source of phosphorus from above rather than below. The external source is probably upwelled bottom water enriched in inorganic phosphorus (e.g., Kazakov, 1937). This also precludes the possibility of regeneration and reflux of phosphorus from the sediments back into the bottom water, due to low oxygen conditions during deposition of the Monterey Formation (e.g., Ingall et al., 1993). An external source of phosphate is also proposed for recent phosphogenetic processes offshore of Baja California, at sites which may be considered as a modern analogue of the Monterey depositional environment (Schuffert et al., 1994).

We therefore postulate the following scenario of phosphogenesis and phosphate accumulation (Fig. 16). Following the rapid deposition of an organic-rich sediment layer, this sediment remained exposed at the seafloor for a longer period of current-induced nondeposition, during which a phosphatic lamina was formed just underneath the sediment-water interface by the transfer of inorganic phosphorus from the seawater into the sediment. This transfer may have been accelerated by bottom-current activity (e.g., Föllmi, 1996). Phosphatic particles may have formed in a similar manner, around agglutinated foraminifera or fecal pellets, for example. The thus-formed phosphates remained pristine if they were untouched by subsequent sediment reworking (Fig. 16A). The formation of condensed phosphates started in the case where the deposition of gravity-flow–derived sediment was associated with erosion and reworking of preexisting sediments, and/or the intervening periods of nondeposition were associated with current-induced winnowing and erosion. In such cases, the thus-formed phosphatic laminae are marked by erosional surfaces and internal discontinuities (Figs. 16B and 16C), and subsequent generations of phosphatic laminae may be in direct contact with each other (stacked or coalesced). Seismic and/or erosive events may have fractured preexisting phosphatic laminae, and the resulting phosphatic lithoclasts may have been concentrated into single layers by winnowing processes or eroded, transported, and redeposited by gravity flows (Figs. 16D and 16E). The condensed intervals are often a product of a combination of these processes and reveal corresponding complex internal stratification patterns (Fig. 16F; Föllmi et al., 1991).

This model is not completely identical with a previously published model (Föllmi and Garrison, 1991), where we assumed that the phosphatic laminae originally represented microbial mats, which were buried by muddy gravity-flow deposits. At that time, we interpreted the rod-like phosphatic particles observed in the phosphatic laminae as phosphatized remains of microbes (Figs. 14A–14C; cf. Reimers et al., 1990). This interpretation is difficult to maintain, because since then, comparable phosphate structures have been shown to form in experiment under sterile conditions (Van Cappellen, 1991). As a

Figure 13. Photomicrographs of condensed phosphatic beds in the Monterey Formation at Naples Beach; scale bar = 1 mm in all images; nonpolarized transmitted light. (A) Phosphatized agglutinated foraminifera in an organic-rich lamina between stacked and partly coalesced phosphatic laminae (Nap 106; cf. Fig. 12B); (B) densely packed phosphatized agglutinated foraminifera (a), peloids, and large, light-colored coprolites (c) (NB 30); (C) phosphatized coprolites (c), peloids, and coated grains (arrows), embedded in an organic-rich matrix (Nap 89); (D) coated phosphatic grains around agglutinated (a) and calcareous benthic foraminifera (b), embedded in a partly phosphatized matrix (NB 26; cf. Fig. 12D); (E) accumulation of partly broken fish debris in an organic-rich red mudstone (Nap 89; cf. Fig. 11E); (F) accumulation of fish debris (f), phosphatized and partly coated agglutinated foraminifera (a), and phosphatized coprolites (c) in a phosphatized matrix (NB 18); (G) fish debris and agglutinated foraminifera embedded in a homogeneous, phosphatized, reddish matrix (NB 31); (H) phosphatized coprolite including fish debris embedded in a phosphatized matrix (NB 31); (I) large, peripherally phosphatized glauconite particles embedded in a phosphatized matrix (Nap 130); (J) phosphatized nodule with a bored and partly eroded surface (arrows), embedded in an entirely phosphatized matrix (NB 9B); (K) phosphatized coprolite and agglutinated foraminifer, both enveloped by a brown phosphate phase and embedded in a phosphatized matrix (NB 26B); (L) phosphatized coprolite enveloped by a brown phosphate phase, which includes an agglutinated foraminifer. Matrix is phosphatized (NB 31); (M) different phosphate generations within a phosphatized nodule (NB 35); (N) succession of phosphatized laminae and lenses of silt-containing sediments. Most interfaces are marked by thin phosphatized envelopes, which are silt free (cf. Fig. 12E); (O) partly fragmented phosphatic lamina; the space created by fragmentation is filled with organic-rich sediment (Nap 95).

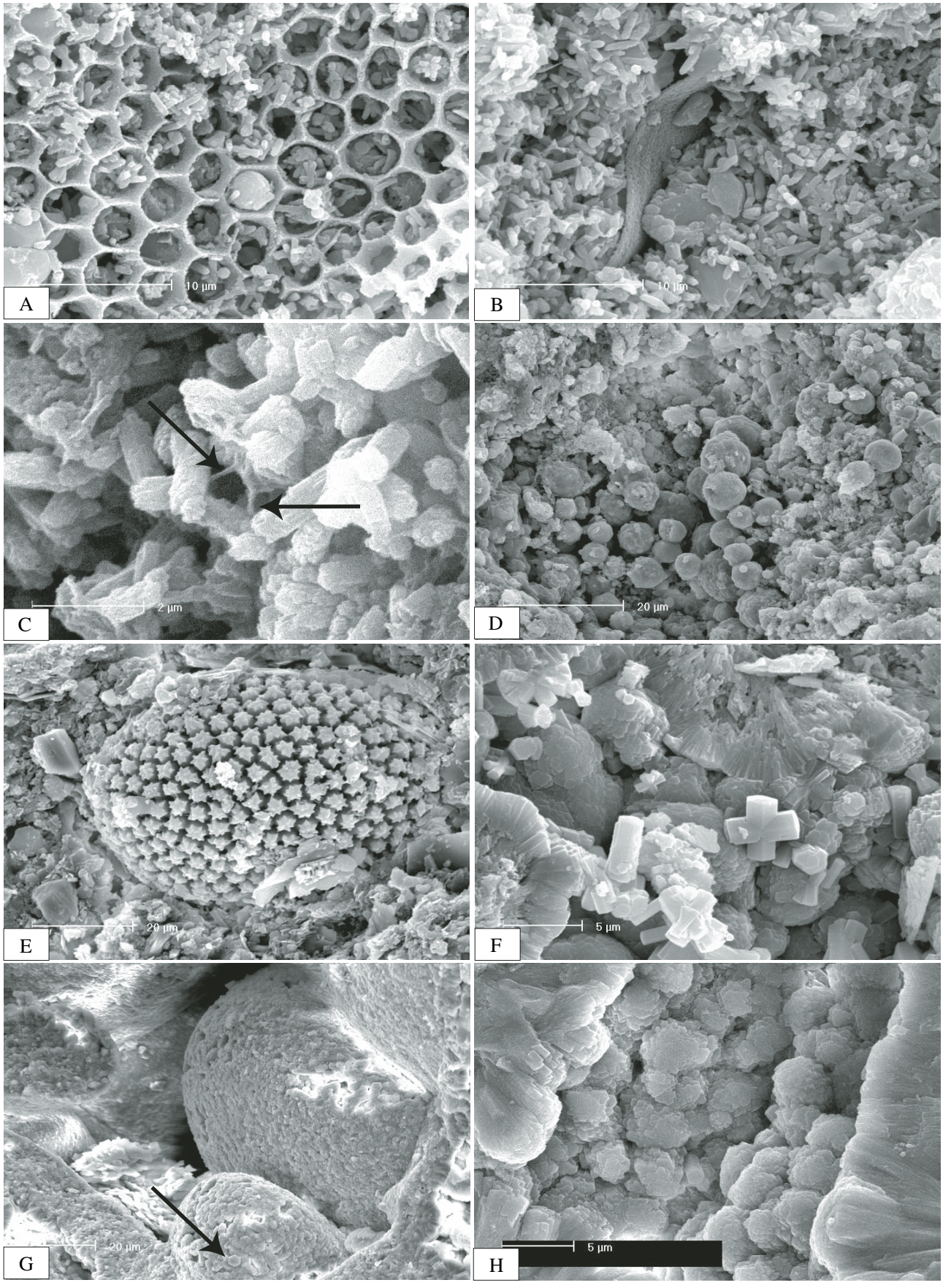
A
10 µm
B
10 µm
C
2 µm
D
20 µm
E
20 µm
F
5 µm
G
20 µm
H
5 µm

consequence, we presently cannot prove that microbes were involved in the process of phosphogenesis even if this may have been likely.

The Monterey Formation in Light of the Monterey Hypothesis

In what they called the Monterey hypothesis, Vincent and Berger (1985) postulated a chain of positive feedback mechanisms in order to explain a major cooling phase, which is documented by an important positive excursion in $\delta^{18}O$ values of benthic foraminifera and presently dated at around 14.5 Ma (e.g., Flower and Kennett, 1994b; Zachos et al., 2001). They assumed that a major glaciation phase in the Antarctic region led to increased latitudinal temperature gradients in the ocean thereby causing reinforced thermohaline oceanic circulation in general and intensified coastal upwelling in the Pacific realm. The associated high productivity rates induced high rates of organic carbon burial, which is documented in formations such as the Californian Monterey Formation and other organic-rich formations around the Pacific rim and indicated by a positive excursion in $\delta^{13}C$ values in benthic foraminifera (from ca. 18–16 Ma; e.g., Flower and Kennett, 1994b). The increased burial of organic carbon triggered the major cooling phase by atmospheric CO_2 drawdown. The onset of organic carbon burial coincided with the beginning of the middle Miocene at around 17.5 Ma, whereas the cooling phase followed with considerable lag. This lag was explained (Vincent and Berger, 1985) by an atmospheric CO_2 threshold level that had to be reached before cooling could occur. The Monterey hypothesis is one of the first hypotheses in which changes in oceanic circulation and climate, the presence of organic-rich sediments, and positive excursions in stable carbon and oxygen isotopes have been bundled into a plausible scenario of climate change by feedback. It has received much attention since its first publication, and a suite of additions and alternative mechanisms have subsequently been proposed.

Using systematic stable isotope evidence in benthic foraminifera, Woodruff and Savin (1989) were able to confirm that major changes in ocean circulation patterns took place during the Miocene. They suggested that the influence of the Tethys on global thermohaline circulation patterns progressively diminished and that from 14.5 Ma onward, North Atlantic deep water formation became more and more important instead, so that by 10 Ma oceanic circulation was very similar to today.

An important and widely discussed alternative was published by Raymo et al. (1988), Raymo and Ruddiman (1992), and Raymo (1994), who identified a phase of increased uplift in the Himalaya as a potential mechanism to increase runoff and nutrient transfer into oceans, thereby enhancing primary productivity and deposition of organic-rich sediments such as those preserved in the Monterey Formation. According to these authors, the drawdown in atmospheric CO_2 was related to intensified chemical weathering in the Himalayan region. This hypothesis was recently challenged both with regard to the timing and importance of the uplift phases (e.g., Hay et al., 2002) as well as to the efficiency of chemical weathering in this region (Derry and France-Lanord, 1996b; France-Lanord and Derry, 1997).

A further twist to the Monterey hypothesis was provided by Hodell and Woodruff (1994), who postulated that the time lag between the onset of organic carbon burial and cooling could be explained by a period of intensified volcanism and the formation of the Columbia River flood basalts, which coincided with the period between 17 and 15 Ma. This volcanic episode may have maintained atmospheric CO_2 levels at higher levels in spite of the phase of organic carbon burial in the Monterey Formation. Several recent studies, however, suggest that atmospheric CO_2 levels were below 280 ppm during most of the Miocene (Pagani et al., 1999; Pearson and Palmer, 2000).

A further intriguing suggestion was recently made by Retallack (2001) and Hay et al. (2002), who observed that the advent of C4 plants and the associate expansion of grasslands during the Miocene may have had an impact on weathering, erosion, and climate through greater efficiency in photosynthetic processes, fixation of water, and weathering of silicates.

Finally, John et al. (2003) suggested that a northward shift in the intertropical convergence zone during the middle Miocene was related to the increased thermal gradient between the North and South Poles. This shift induced increased rainfall in formerly drier areas, which in turn led to increased weathering rates.

Whereas the mechanisms leading to middle Miocene climate change are still a matter of debate, the assumption that organic carbon burial rates were high at the depositional sites of the Monterey Formation during the positive $\delta^{13}C$ excursion has not been questioned until recently. Isaacs (2001) and John et al. (2002) were the first to show that organic carbon accumulation rates in the Monterey Formation are modest. Also in this study, we show that in spite of the generally high TOC values (up to 22 wt%) observed in the Monterey Formation at Naples Beach, the corresponding organic carbon accumulation rates are rather low in comparison to those of modern high-productivity areas. Furthermore, organic carbon accumulation continued well beyond the climate cooling phase, and a direct correlation between organic-carbon burial and climate change is not evident (cf. Isaacs, 2001). Also the burial rates of phosphorus, an essential nutrient, did not dramatically change prior to 13 Ma. A similar observation was made for the section at El Capitan State Beach (covering the period >16.3 to <10.8 Ma), where organic carbon accumulation rates only started to rise from 14.5 Ma onward (John et al., 2002).

Condensation and phosphogenesis in association with the deposition of organic-rich sediments is a widely observed facies in sections and well logs of the Monterey Formation from different basins (e.g., Garrison et al., 1987, 1990). This may imply that moderate organic carbon burial rates are common in a larger part of the Monterey Formation. This does not mean that high organic carbon burial rates are excluded for the Monterey Formation (and for related formations around the Pacific rim), but so far we have no positive evidence for this. This may in turn mean that the Monterey Formation did not necessarily represent a major sink of organic carbon burial during the middle Miocene. If this

Figure 14. Scanning electron micrographs of phosphatic laminae, nodules, and condensed horizons in the Monterey Formation at Naples Beach. (A) Light-colored phosphatic lamina (Nap 13); rod-like phosphatic corpuscles infilling the pore space of a diatom; (B) light-colored phosphatic lamina (Nap 13); phosphate is present in the form of rod-like structures; (C) close-up of the rod-like phosphatic corpuscules in a light-colored phosphatic lamina with filament structures between the phosphates (arrows) (Nap 19); (D) light-colored phosphatic nodule build-up of phosphatic microspheres (Nap 80); (E) light-colored phosphatic nodule (Nap 80); pores of a diatom were filled in by phosphate before the diatom dissolved; (F) condensed phosphatic horizon (Nap 89; cf. Fig. 11E); pore enveloped by crystalline, radiating, and globular phosphate, and isolated hexagonal idiomorphic phosphate crystals, which are partly cross twinned; (G) condensed phosphatic horizon (Nap 89; cf. Fig. 11E); surfaces composed of crystalline phosphate (partly with hexagonal crystals [arrow]) of phosphatic nodules; (H) condensed phosphatic horizon (Nap 89; cf. Fig. 11E); crystalline cauliflower-like phosphate lining a pore space.

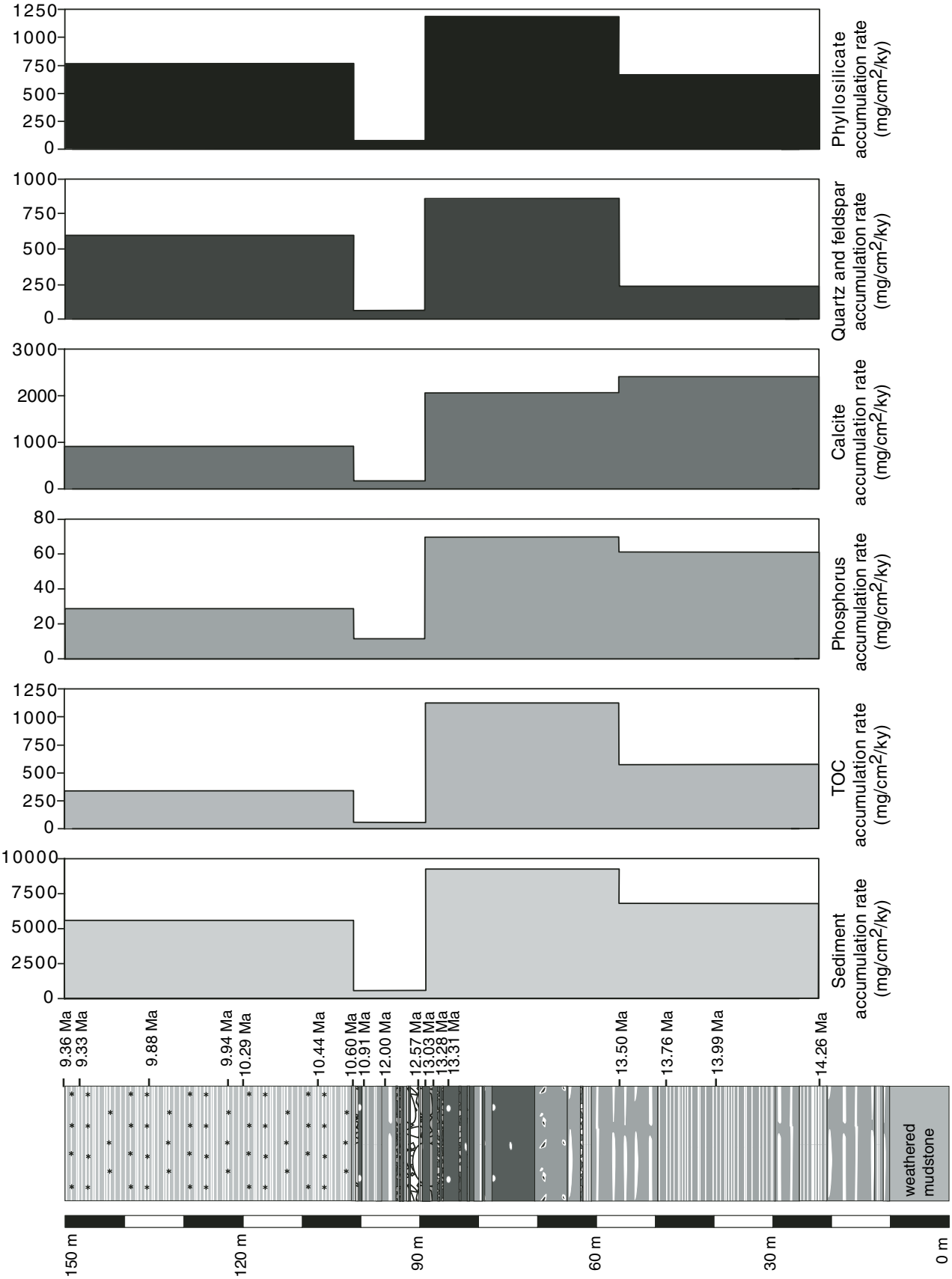

Figure 15. Accumulation rates in mg/cm²/k.y. for total sediment, TOC, phosphorus, calcite, quartz and feldspar, and phyllosilicates calculated and averaged for four intervals.

TABLE 5. HOLOCENE TOTAL ORGANIC CARBON (TOC) MASS ACCUMULATION RATES (MAR) IN mg/cm^2/k.y. IN A SELECTION OF MODERATE- TO HIGH-PRODUCTIVITY SITES, COMPARED TO TOC MAR OF THE MONTEREY FORMATION

Core	TOC MAR	Average	Reference
Peru margin: upper slope at approx. 15°S	9000–12000	10500	Reimers and Suess (1983)
Peru margin: 7706–39	500–3300	3000	Reimers and Suess (1983))
Peru margin: 7706–41	1400–6300	4000	Reimers and Suess (1983)
Peru margin: 7706–04	1100–2000	1500	Reimers and Suess (1983)
Peru margin: 7706–36	900–1600	1300	Reimers and Suess (1983)
Peru margin: ODP Site 112–680	800–3000	2000	Tamburini (2001)
Eastern tropical Atlantic: ODP Site 108–658	200–500	300	Tamburini (2001)
Oman margin: ODP Site 117–724	100–400	250	Tamburini (2001)
Japan Sea: ODP 128–798	100–400	250	Tamburini (2001)
South China Sea: ODP Site 184–1144	150–500	250	Tamburini (2001)
Monterey Formation, Naples Beach	55–1130	310	This paper
Monterey Formation, El Capitan St. Beach	40–390	150	John et al. (2002)

is indeed so, alternative mechanisms are needed to explain the positive shift in $\delta^{13}C$.

An early compilation extracted from the Deep Sea Drilling Project (DSDP) records by Southam and Hay (1981) shows a major increase in organic carbon burial rates in general during the middle Miocene. This increase was confirmed for the same period in a model by Derry and France-Lanord (1996a), where they used a stable carbon isotope mass balance. Furthermore, Southam and Hay (1981) and Derry and France-Lanord (1996a) showed that the organic carbon burial rates continued to increase up to the present. Along the same lines, France-Lanord and Derry (1997) suggested that Himalayan erosion and the associated increase in sedimentation rates in the northern part of the Indian Ocean (Bengal Fan and Ganges-Brahmaputra delta) may have contributed considerably to the general increase in organic carbon burial. This observation is consistent with the data published by Hay (1998) and Hay et al. (2002), who observed that during the last 15 Ma the sediment flux increased by ~50% on a global scale.

During the Miocene, organic carbon burial was also important on the continent. Major brown coal deposits are known from different regions in Europe and the United States, from Greenland, Turkey, India, Russia, Japan, China, Thailand, Indonesia, Australia, and New Zealand. The onset of lignite deposition in NW Germany, for example, started at around 18 Ma, near the onset of the positive $\delta^{13}C$ excursion (Utescher et al., 2000).

It seems therefore likely that an important trigger of the positive $\delta^{13}C$ excursion is associated with enhanced organic carbon burial on the continent and in marine depocenters. The positive $\delta^{13}C$ excursion ended, however, at around 16–15 Ma (e.g., Flower and Kennett, 1994b), whereas organic carbon burial rates continued to increase. This suggests that the increase in organic carbon burial alone may not have been sufficient in driving the positive $\delta^{13}C$ excursion. Other factors, such as the disappearance of shallow-water carbonate platforms (platform drowning; Schlager, 1981) may have been involved as well. Changes in shallow-water carbonate production have been shown to be influential in driving stable isotope signatures (e.g., Weissert et al., 1998) and drowning or important backstepping of carbonate platforms has been documented for different platforms during this period; for instance in the South China Sea (between 21.2 and 17.9 Ma: Erlich et al., 1990); at the early-middle Miocene boundary (Fulthorpe and Schlanger, 1989); the Mediterranean area (between 20 and 16 Ma: Mutti et al., 1997; between 17.5 and 16–15 Ma: Brandano and Corda, 2002); and the Caribbean (24–16 Ma: Edinger and Risk, 1994).

The disappearance of carbonate platforms may have been related to the enhanced detrital and associated nutrient flux rates (cf. Mutti et al., 1997; Brandano and Corda, 2002). A further expression of this phenomenon may be sought in the widespread occurrence of phosphate-rich sediments that date from this period. Indeed, the early to middle Miocene is a period of increased phosphorus burial rates, phosphogenesis, and the formation of economically viable phosphorite deposits (Cook and McElhinny, 1979; Föllmi, 1995), such as are found in South Carolina and Florida (Riggs, 1979, 1984; Riggs and Sheldon, 1990; Compton et al., 1990, 1993).

CONCLUSIONS

The Miocene Monterey Formation of the central Californian borderland is regarded as a model formation for the study of sedimentation processes along an active margin, organic-carbon accumulation and phosphogenesis related to coastal upwelling, early diagenetic formation of dolomite and transformation of biosilica, and its relation to climate change during the middle Miocene (the Monterey hypothesis, Vincent and Berger, 1985). Our analysis of the mineralogy, sedimentary structures, organic matter, phosphates, and nannofossils in the organic-carbon and phosphate-rich part of the Monterey Formation at Naples Beach allows us to formulate the following conclusions.

1. The common presence of sedimentary structures such as slumps, local unconformities, erosive surfaces, and reworked clasts points to the importance of bottom-current activity and gravity-flow deposition, and we assume that a considerable portion of the organic-rich mud has been deposited under the influence of gravity-flow deposition.

2. Organic-carbon accumulation at this site is therefore the result of the balance between gravity-flow deposition and subsequent erosion by current activity and high-energy events such as seismic events rather than by the deposition of suspended organic matter.

3. Strontium isotopes measured in a selection of phosphatic materials do not provide stratigraphically meaningful ages; this may be due to the widespread occurrence of volcanic ash layers, which may have contaminated the strontium isotope signal in the phosphate.

4. A new age model based on calcareous nannofossils allows us to quantify organic-carbon accumulation rates, which varied between 55 and 1130 mg/cm^2/k.y. These rates are considered to be modest: the average rate corresponds to ~8% of the organic-carbon accumulation rate actually found in the high-productivity area offshore of Peru.

5. Given these rather low rates, the high average TOC values (between 6 and 12 wt% outside the condensed interval) appear to be the product of good preservation conditions, which overruled the negative effects related to periods of nondeposition and occasional sediment reworking and removal on organic-matter preservation. We suggest that early diagenetic sealing of the sediments by phosphatic laminae may have been advantageous for organic-carbon preservation, besides the more commonly invoked conditions such as low-oxygen conditions.

6. Phosphogenesis and the formation of phosphatic laminae was a very early diagenetic process, which took place in the uppermost centimeters of the sediment, close to the sediment-water interface. Once formed, the phosphatic laminae were often affected by subsequent processes, such as fracturing, slumping, winnowing, erosion, and bioturbation.

7. The formation of condensed phosphatic beds is the product of highly dynamic sedimentation processes, which were induced by a combination of current and seismic activity. The result is stacked and coalesced phosphatic laminae, fractured phosphate layers, winnowed phosphate-rich layers, and redeposited conglomeratic layers. Most condensed beds in the Monterey Formation are a composite of these different stratification types.

8. The Monterey Formation at Naples Beach is highly enriched in phosphorus relative to organic carbon. Since the Redfield ratio is preserved in the mudstone of a selected representative sample, we suggest that this is due to an external source of phosphorus (seawater). This precludes the regeneration of organic phosphorus by early diagenetic decomposition of organic matter as an internal source of phosphorus and also a potential reflux of phosphorus from the sediment into the bottom water related to low-oxygen conditions.

9. Changes in continental weathering regimes induced by climate change, the advent of C4 plants, and the spreading of grasslands, and the increasing importance of the Himalaya and other mountain chains considerably increased sedimentary fluxes and organic-burial in near-continental depocenters. The increased flux of detrital sediments and associated nutrients may have been responsible for the widespread backstepping and drowning of shallow-water platforms during the early and early middle Miocene, and both the increase in organic-carbon burial as well as the decrease in shallow-water carbonate production may have been involved in the positive shift in late early to early middle Miocene $\delta^{13}C$. At the same time, conditions were appropriate for the widespread formation of phosphate-rich sediments.

10. The formation of important and widespread lignite deposits on the continent during the Miocene points to a further important carbon sink that may have been implied in atmospheric CO_2 drawdown and cooling.

11. For the Monterey Formation at Naples Beach, a direct correlation between organic-carbon burial and climate change is not evident. Phosphorus burial rates did not dramatically change prior to 13 Ma. In spite of the generally high TOC values, the sediments of the Monterey Formation may not represent an important sink for organic carbon during the middle Miocene, which would deprive the Monterey hypothesis of its main witness.

ACKNOWLEDGMENTS

We would like to thank Robert E. Garrison, Rick Behl, Kurt Grimm, Caroline Isaacs, John Barron, Miriam Kastner, Claire Reimers, Ahmed El-Shistawy,

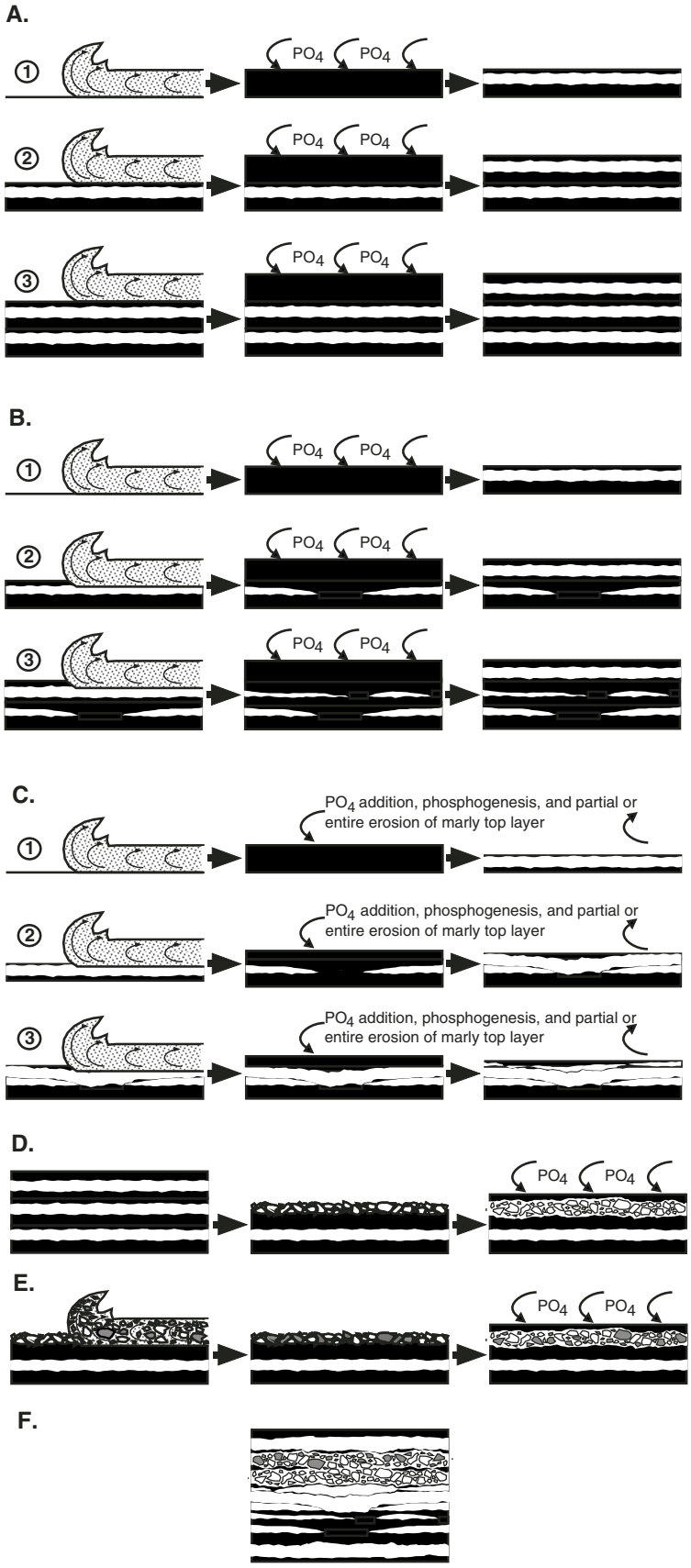

Figure 16. Model for the formation of phosphatic laminae and condensed and allochthonous phosphatic beds in the Monterey Formation at Naples Beach.

Pedro Gonzales, and Lisa White for numerous discussions, help in the field, and logistical support; Gene Gonzales, Gérard Magranville, and André Villard for the preparation of excellent thin sections from delicate sample material; and Massoud Dadras and Michèle Vliemant for assistance at the SEM and ESEM. Furthermore, we would like to acknowledge the Swiss National Science Foundation and the Matthey-Dupraz foundation for financial support during different stages of this research. The suggestions of two anonymous reviewers, Wolfgang Schlager, associate editor, and Yildirim Dilek, editor of GSA Bulletin improved the manuscript greatly.

REFERENCES CITED

Adatte, T., Stinnesbeck, W., and Keller, G., 1996, Lithostratigraphic and mineralogic correlations of near K/T boundary clastic sediments in northeastern Mexico, *in* Ryder, G., Fastovsky, D., Gartner, S., eds., Implications for origin and nature of deposition: Geological Society of America Special Paper 307, p. 211–226.

Anderson, L.D., and Delaney, M.L., 2000, Sequential extraction and analysis of phosphorus in marine sediments: Streamlining of the SEDEX procedure: Limnology and Oceanography, v. 45, p. 509–515.

Arends, R.G., and Blake, G.H., 1986, Biostratigraphy and paleoecology of the Naples Bluff coastal section based on diatoms and benthic foraminifera, *in* Casey, R.E., and Barron, J.A., eds., Siliceous Microfossils and Microplankton of the Monterey Formation and Modern Analogs: Society of Economic Petrologists and Paleontologists, Pacific Section, Special Publication 45, p. 121–135.

Badertscher, C., 2000, La Formation de Monterey (Miocène) à "Naples Beach," Santa Barbara, Californie: Une approche sédimentologique, mineralogique et géochimique [diploma thesis]: Neuchâtel, University of Neuchâtel, 38 p.

Baker, P.A., and Kastner, M., 1981, Constraints on the formation of sedimentary dolomite: Science, v. 213, p. 214–216.

Barron, J.A., 1986a, Paleoceanographic and tectonic controls on deposition of the Monterey Formation and related siliceous rocks in California: Palaeogeography, Palaeoclimatology, Palaeoecology, v. 53, p. 27–45, doi: 10.1016/0031-0182(86)90037-4.

Barron, J.A., 1986b, Updated diatom biostratigraphy for the Monterey Formation of California, *in* Casey, R.E., and Barron, J.A., eds., Siliceous Microfossils and Microplankton of the Monterey Formation and Modern Analogs: Society of Economic Petrologists and Paleontologists, Pacific Section, Special Publication 45, p. 105–119.

Barron, J.A., and Isaacs, C.M., 2001, Updated chronostratigraphic framework for the California Miocene, *in* Isaacs, C.M., and Rullkötter, J., eds., The Monterey Formation: From Rocks to Molecules: New York, Columbia University Press, p. 393–395.

Behar, F., Beaumont, V., and Penteado, H.L.D., 2001, Rock-Eval 6 technology: Performances and developments: Oil & Gas Science and Technology, v. 56, p. 111–134.

Behl, R.J., 1992, Chertification in the Monterey Formation of California and deep-sea sediments of the West Pacific [Ph.D. thesis]: Santa Cruz, University of California, 287 p.

Behl, R.J., 1999, Since Bramlette (1946): The Miocene Monterey Formation of California revisited, *in* Moores, E.M., Sloan, D., and Stout, D.L., eds., Classic Cordilleran Concepts: A View from California: Geological Society of America Special Paper 338, p. 301–313.

Behl, R.J., and Garrison, R.E., 1994, The origin of chert in the Monterey Formation of California (USA), *in* Iijima, A., Abed, A.M., and Garrison, R.E., eds., Siliceous, Phosphatic, and Glauconitic Sediments of the Tertiary and Mesozoic: 29th International Geological Congress, Proceedings, Part C: Zeist, The Netherlands, VSP International Publishers, p. 101–132.

Blake, G.H., 1981, Biostratigraphic relationship of Neogene benthic foraminifera from the southern California outer continental borderland to the Monterey Formation, *in* Garrison, R.E., and Douglas, R.G., eds., The Monterey Formation and Related Siliceous Rocks of California: Society of Economic Petrologists and Paleontologists, Pacific Section, Special Publication 15, p. 1–14.

Blake, G.H., 1994, Detailed biostratigraphy and paleoenvironmental interpretation of the Naples Bluff section, *in* Hornafius, J.S., ed., Field Guide to the Monterey Formation between Santa Barbara and Gaviota, California: American Association of Petroleum Geologists, Pacific Section Field Guide GB72, p. 17–28.

Bramlette, M.N., 1946, The Monterey Formation of California and the origin of its siliceous rocks: U.S. Geological Survey Professional Paper 212, 57 p.

Brandano, M., and Corda, L., 2002, Nutrients, sea level and tectonics: Constraints for the facies architecture of a Miocene carbonate ramp in central Italy: Terra Nova, v. 14, p. 257–262, doi: 10.1046/j.1365-3121.2000.00419.x.

Burns, S.J., and Baker, P.A., 1987, A geochemical study of dolomite in the Monterey Formation, California: Journal of Sedimentary Petrology, v. 57, p. 128–139.

Chaika, C., and Williams, L.A., 2001, Density and mineralogy variations as a function of porosity in Miocene Monterey Formation oil and gas reservoirs in California: American Association of Petroleum Geologists Bulletin, v. 85, p. 149–167.

Chang, A.S., and Grimm, K.A., 1999, Speckled beds: Distinctive gravity-flow deposits in finely laminated diatomaceous sediments, Miocene Monterey Formation, California: Journal of Sedimentary Research, v. 69, p. 122–134.

Chang, A.S., Grimm, K.A., and White, L.D., 1998, Diatomaceous sediments from the Miocene Monterey Formation, California: A lamina-scale investigation of biological, ecological, and sedimentary processes: Palaios, v. 13, p. 439–458.

Compton, J.S., 1988, Sediment composition and precipitation of dolomite and pyrite in the Neogene Monterey and Sisquoc Formations, Santa Maria Basin area, California, *in* Shukla, V., and Baker, P.A., eds., Sedimentology and geochemistry of Dolostones: Society of Economic Petrologists and Paleontologists Special Publication 22, p. 53–65.

Compton, J.S., 1991a, Porosity reduction and burial history of siliceous rocks from the Monterey and Sisquoc Formation, Point Pedernalis area, California: Geological Society of America Bulletin, v. 103, p. 625–636, doi: 10.1130/0016-7606(1991)1032.3.CO;2.

Compton, J.S., 1991b, Origin and diagenesis of clay minerals in the Monterey Formation, Santa Maria Basin area, California: Clay and Clay Minerals, v. 39, p. 449–466.

Compton, J.S., Snyder, S.W., and Hodell, D.A., 1990, Phosphogenesis and weathering of shelf sediments from the southeastern United States: Implications for Miocene $\delta^{13}C$ excursions and global cooling: Geology, v. 18, p. 1227–1230, doi: 10.1130/0091-7613(1990)0182.3.CO;2.

Compton, J.S., Hodell, D.A., Garrido, J.R., and Mallinson, D.J., 1993, Origin and age of phosphorite from the south-central Florida platform: Relation of phosphogenesis to sea-level fluctuations and $\delta^{13}C$ excursions: Geochimica et Cosmochimica Acta, v. 57, p. 131–146, doi: 10.1016/0016-7037(93)90474-B.

Cook, P.J., and McElhinny, M.W., 1979, A re-evaluation of the spatial and temporal distribution of sedimentary phosphate deposits in the light of plate tectonics: Economic Geology and the Bulletin of the Society of Economic Geologists, v. 74, p. 315–330.

De Kaenel, E., and Villa, G., 1996, Oligocene–Miocene calcareous nannofossil bostratigraphy and paleoecology from the Ibera abyssal plain, *in* Whitmarsh, R.B., Sawyer, D.S., Klaus, A., and Masson, D.G., eds., Proceedings of the Ocean Drilling Program, Scientific Results, v. 149, p. 79–145.

De Paolo, D.J., and Finger, K.L., 1991, High-resolution strontium-isotope stratigraphy and biostratigraphy of the Miocene Monterey Formation, central California: Geological Society of America Bulletin, v. 103, p. 112–124, doi: 10.1130/0016-7606(1991)1032.3.CO;2.

Derry, L.A., and France-Lanord, C., 1996a, Neogene growth of the sedimentary organic carbon reservoir: Paleoceanography, v. 11, p. 267–275, doi: 10.1029/95PA03839.

Derry, L.A., and France-Lanord, C., 1996b, Neogene Himalayan history and river $^{87}Sr/^{86}Sr$ impact on the marine Sr record: Earth and Planetary Science Letters, v. 142, p. 59–74, doi: 10.1016/0012-821X(96)00091-X.

Dzulynski, S., 1996, Erosional and deformational structures in single sedimentary beds: A genetic commentary: Annales Societatis Geologorum Poloniae, v. 66, p. 101–189.

Echols, R.J., 1994, Biostratigraphy of the Luisian and Mohnian stages between Santa Barbara and Gaviota, California, *in* Hornafius, J.S., ed., Field Guide to the Monterey Formation between Santa Barbara and Gaviota, California: American Association of Petroleum Geologists, Pacific Section Field Guide GB72, p. 29–44.

Edinger, A.N., and Risk, M.J., 1994, Oligocene-Miocene extinction and geographic restriction of Caribbean corals: Roles of turbidity, temperature, and nutrients: Palaios, v. 9, p. 578–598.

Eichhubl, P., and Boles, J.R., 2000, Focused fluid flow along faults in the Monterey Formation, coastal California: Geological Society of America Bulletin, v. 112, p. 1667–1679, doi: 10.1130/0016-7606(2000)1122.0.CO;2.

Erlich, R.N., Barrett, S.F., and Ju, G.B., 1990, Seismic and geologic characteristics of drowning events on carbonate platforms: American Association of Petroleum Geology Bulletin, v. 74, p. 1523–1537.

Espitalié, J., Deroo, G., and Marquis, F., 1985, La pyrolyse Rock-Eval et ses applications: Institut Français du Pétrole, Revue, v. 40, p. 563–579.

Filippelli, G.M., and Delaney, M.L., 1992, Similar phosphorus fluxes in ancient phosphorite deposits and a modern phosphogenic environment: Geology, v. 20, p. 709–712, doi: 10.1130/0091-7613(1992)0202.3.CO;2.

Filippelli, G.M., and Delaney, M.L., 1994, Phosphogenesis and the controls on phosphorus accumulation in continental margin sediments, *in* Iijima, A., Abed, A.M., and Garrison, R.E., eds., Siliceous, Phosphatic, and Glauconitic sediments of the Tertiary and Mesozoic: 29th International Geological Congress, Proceedings, Part C: Zeist, The Netherlands, VSP International Publishers, p. 189–204.

Filippelli, G.M., and Delaney, M.L., 1995, Phosphogenesis geochemistry, diagenesis, and mass balances of the Miocene Monterey Formation at Shell Beach, California, *in* Keller, M.A., ed., Evolution of sedimentary basins/onshore oil and gas investigations—Santa Maria province: U.S. Geological Survey Bulletin, p. G1–G11.

Filippelli, G.M., and Delaney, M.L., 1996, Phosphorus geochemistry of equatorial Pacific sediments: Geochimica et Cosmochimica Acta, v. 60, p. 1479–1495, doi: 10.1016/0016-7037(96)00042-7.

Filippelli, G.M., Delaney, M.L., Garrison, R.E., Omarzai, S.K., and Behl, R.J., 1994, Phosphorus accumulation rates in a Miocene low oxygen basin: The Monterey Formation (Pismo Basin), California: Marine Geology, v. 116, p. 419–430, doi: 10.1016/0025-3227(94)90055-8.

Flower, B.P., and Kennett, J.P., 1993, Relations between Monterey Formation deposition and middle Miocene global cooling: Naples Beach section, California: Geology, v. 21, p. 877–880, doi: 10.1130/0091-7613(1993)0212.3.CO;2.

Flower, B.P., and Kennett, J.P., 1994a, Oxygen and carbon isotopic stratigraphy of the Monterey Formation at Naples Beach, California, *in* Hornafius, J.S., ed., Field Guide to the Monterey Formation Between Santa Barbara and Gaviota, California: American Association of Petroleum Geology, Pacific Section Field Guide GB72, p. 59–66.

Flower, B.P., and Kennett, J.P., 1994b, The middle Miocene climatic transition: East Antarctica ice sheet development, deep ocean circulation and global carbon cycling: Palaeogeography, Palaeoclimatology, Palaeoecology, v. 108, p. 537–555, doi: 10.1016/0031-0182(94)90251-8.

Föllmi, K.B., 1995, 160 m.y. record of marine sedimentary phosphorus burial: Coupling of climate and continental weathering under greenhouse and icehouse conditions: Geology, v. 23, p. 859–862, doi: 10.1130/0091-7613(1995)0232.3.CO;2.

Föllmi, K.B., 1996, The phosphorus cycle, phosphogenesis and marine phosphate-rich deposits: Earth-Science Reviews, v. 40, p. 55–124, doi: 10.1016/0012-8252(95)00049-6.

Föllmi, K.B., and Garrison, R.E., 1991, Phosphatic sediments, ordinary or extraordinary deposits? The example of the Miocene Monterey Formation (California),

in Müller, D.W., McKenzie, J.A., and Weissert, H., eds., Controversies in Modern Geology: London, Academic Press, p. 55–84.

Föllmi, K.B., and Grimm, K.A., 1990, Doomed pioneers: Gravity-flow deposition and bioturbation in marine dysaerobic environments: Geology, v. 18, p. 1069–1072, doi: 10.1130/0091-7613(1990)0182.3.CO;2.

Föllmi, K.B., Garrison, R.E., and Grimm, K.A., 1991, Stratification in Phosphatic Sediments: Illustration from the Neogene of California, *in* Einsele, G., Ricken, W., and Seilacher, A., eds., Cycles and Events in Stratigraphy: Berlin, Springer-Verlag, p. 492–507.

France-Lanord, C., and Derry, L.A., 1997, Organic carbon burial forcing of the carbon cycle from Himalayan erosion: Nature, v. 390, p. 65–67, doi: 10.1038/36324.

Fulthorpe, G.S., and Schlanger, S.O., 1989, Paleo-oceanographic and tectonic settings of early Miocene reefs and associated carbonates of offshore southeast Asia: Association of American Petrologists, Bulletin, v. 73, p. 729–756.

Galloway, J.M., 1998, Chronology of petroleum exploration and development in the Santa Barbara Channel area, offshore southern California, *in* Kunitomi, D.S., Hopps, T.E., and Galloway, J.M., eds., Structure and Petroleum Geology, Santa Barbara Channel, California: American Association of Petroleum Geologists, Pacific Section, and Coast Geological Society, Miscellaneous Publication 46, p. 1–11.

Garrison, R.E., and Douglas, R.G., eds., 1981, The Monterey Formation and Related Siliceous Rocks of California: Society of Economic Petrologists and Paleontologists, Pacific Section, Special Publication 15, 327 p.

Garrison, R.E., Kastner, M., and Zenger, D.H., eds., 1984, Dolomites of the Monterey Formation and other organic-rich units: Society of Economic Petrologists and Paleontologists, Pacific Section, Special Publication 41, 215 p.

Garrison, R.E., Kastner, M., and Kolodny, Y., 1987, Phosphorites and phosphatic rocks in the Monterey Formation and related Miocene units, coastal California, *in* Ingersoll, R.V., and Ernst, W.G., eds., Cenozoic Basin Development in Coastal California: Rubey Volume 6: Englewood Cliffs, New Jersey, Prentice-Hall, p. 348–381.

Garrison, R.E., Kastner, M., and Reimers, C.E., 1990, Miocene phosphogenesis in California, *in* Burnett, W.C., and Riggs, S.R., eds., Phosphate Deposits of the World, vol. 3, Neogene to Modern Phosphorites: Cambridge, Cambridge University Press, p. 285–299.

Garrison, R.E., Hoppie, B.W., and Grimm, K.A., 1994, Phosphates and dolomites in coastal upwelling sediments of the Peru margin and the Monterey Formation (Naples Beach section), California, *in* Hornafius, J.S., ed., Field Guide to the Monterey Formation between Santa Barbara and Gaviota, California: American Association of Petroleum Geologists, Pacific Section Field Guide GB72, p. 67–84.

Graham, S.A., 1987, Tectonic controls on petroleum occurrence in central California, *in* Ingersoll, R.V., and Ernst, W.G., eds., Cenozoic Basin Development in Coastal California: Rubey Volume 6: Englewood Cliffs, New Jersey, Prentice-Hall, p. 407–426.

Graham, S.A., and Williams, L.A., 1985, Tectonic, depositional, and diagenetic history of Monterey Formation (Miocene), central San Joaquin Basin, California: American Association of Petroleum Geologists Bulletin, v. 69, p. 385–411.

Grimm, K.A., and Föllmi, K.B., 1994, Doomed pioneers: Allochthonous crustacean tracemakers in anaerobic basinal strata, Oligo-Miocene San Gregorio Formation, Baja California Sur, Mexico: Palaios, v. 9, p. 313–334.

Grimm, K.A., and Orange, D.L., 1997, Synsedimentary fracturing, fluid migration, and subaqueous mass wasting: Intrastratal microfractured zones in laminated diatomaceous sediments, Miocene Monterey Formation, California, USA: Journal of Sedimentary Research, v. 67, p. 601–613.

Gross, M.R., 1995, Fracture partitioning, failure mode as as function of lithology in the Monterey Formation of coastal California: Geological Society of America Bulletin, v. 107, p. 779–792, doi: 10.1130/0016-7606(1995)1072.3.CO;2.

Hay, W.W., 1998, Detrital sediment fluxes from continents to oceans: Chemical Geology, v. 145, p. 287–323, doi: 10.1016/S0009-2541(97)00149-6.

Hay, W.W., Soeding, E., DeConto, R.M., and Wold, C.N., 2002, The late Cenozoic uplift—Climate change paradox: International Journal of Sciences, v. 91, p. 746–774, doi: 10.1007/s00531-002-0263-1.

Hilgen, F.J., Krijgsman, W., Raffi, I., Turco, E., and Zachariasse, W.J., 2000, Integrated stratigraphy and astronomical calibration of the Serravalian/Tortonian boundary section at Monte Gibliscemi (Sicily, Italy): Marine Micropaleontology, v. 38, p. 181–211, doi: 10.1016/S0377-8398(00)00008-6.

Hodell, D.A., and Woodruff, F., 1994, Variations in the strontium isotopic ratio of seawater during the Miocene: Stratigraphic and geochemical implications: Paleoceanography, v. 9, p. 405–426, doi: 10.1029/94PA00292.

Hoppie, B., and Garrison, R.E., 2001, Miocene phosphate accumulation in the Cuyama Basin, Southern California: Marine Geology, v. 177, p. 353–380, doi: 10.1016/S0025-3227(01)00169-4.

Hoppie, B., and Garrison, R.E., 2002, The Cuyama strike-slip basin, California, USA: An examplar of contrasting syntectonic and post-tectonic strata: Journal of Sedimentary Research, v. 72, p. 268–287.

Hornafius, J.S., ed., 1994, Field Guide to the Monterey Formation between Santa Barbara and Gaviota, California: American Association of Petroleum Geologists, Pacific Section, Field Guide GB72, 123 p.

Ingall, E.D., Bustin, R.M., and Van Cappellen, P., 1993, Influences of water column anoxia on the burial and preservation of carbon and phosphorus in marine shales: Geochimica et Cosmochimica Acta, v. 57, p. 303–316, doi: 10.1016/0016-7037(93)90433-W.

Ingle, J.C.J., 1980, Cenozoic paleobathymetry and depositional history of selected sequences within the southern California continental borderland, *in* Sliter, W., ed., Studies in Micropaleontology: Washington, D.C., Cushman Foundation for Foraminiferal Research, Special Publication 19, p. 163–195.

Isaacs, C.M., 1981a, Outline of diagenesis in the Monterey Formation examined laterally along the Santa Barbara coast, California, *in* Isaacs, C.M., ed., Guide to the Monterey Formation in the California Coastal area, Ventura to San Luis Obispo: American Association of Petroleum Geologists, Pacific Section, Special Publication 52, p. 25–38.

Isaacs, C.M., 1981b, Lithostratigraphy of the Monterey Formation, Goleta to Point Conception, Santa Barbara coast, California, *in* Isaacs, C.M., ed., Guide to the Monterey Formation in the California Coastal area, Ventura to San Luis Obispo: American Association of Petroleum Geologists, Pacific Section, Special Publication 52, p. 9–24.

Isaacs, C.M., 1981c, Porosity reduction during diagenesis of the Monterey Formation, Santa Barbara coastal area, California, *in* Garrison, R.E., and Douglas, R.G., eds., 1981, The Monterey Formation and related siliceous rocks of California: Society of Economic Petrologists and Paleontologists, Pacific Section, Special Publication 15, p. 257–271.

Isaacs, C.M., 1982, Influence of rock composition on the kinetics of silica phase changes in the Monterey Formation, Santa Barbara area, California: Geology, v. 10, p. 304–308.

Isaacs, C.M., 1984, Hemipelagic deposits in a Miocene basin, California: Toward a model of lithologic variation and sequence, *in* Stow, D.A.V., and Piper, D.J.W., eds., Fine-grained sediments: Deep-water processes and facies: Geological Society [London] Special Publication 4, p. 481–496.

Isaacs, C.M., 1985, Abundance versus rates of accumulation in fine-grained strata of the Miocene Santa Barbara basin, California: Geo-Marine Letters, v. 5, p. 25–30.

Isaacs, C.M., 2001, Depositional framework of the Monterey formation, California, *in* Isaacs, C.M., and Rullkötter, J., eds., The Monterey Formation: From Rocks to Molecules: New York, Columbia University Press, p. 1–30.

Isaacs, C.M., and Garrison, R.E., eds., 1983, Petroleum Generation and Occurrence in the Miocene Monterey Formation, California: Los Angeles, Society of Economic Petrologists and Paleontologists, Pacific Section Special Publication, 228 p.

Isaacs, C.M., and Petersen, N.F., 1987, Petroleum in the Miocene Monterey Formation, California, *in* Hein, J.R., ed., Siliceous Sedimentary Rock-Hosted Ores and Petroleum: Evolution of Ore Fields: New York, Van Nostrand Reinhold, p. 83–116.

Isaacs, C.M., and Rullkötter, J., eds., 2001, The Monterey Formation: From Rocks to Molecules: New York, Columbia University Press, 608 p.

Isaacs, C.M., Pisciotto, K.A., and Garrison, R.E., 1983, Facies and diagenesis of the Miocene Monterey Formation, California: A summary, *in* Iijima, A., Hein, J.R., and Siever, R., eds., Siliceous Deposits in the Pacific Region: Amsterdam, Elsevier, Developments in Sedimentology, v. 36, p. 247–282.

Jacobs, E., Weissert, H., Shields, G., and Stille, P., 1996, The Monterey event in the Mediterranean: A record from shelf sediments of Malta: Paleoceanography, v. 11, p. 717–728, doi: 10.1029/96PA02230.

John, C.M., Föllmi, K.B., de Kaenel, E., Adatte, T., Steinmann, P., and Badertscher, C., 2002, Carbonaceous and phosphate-rich sediments of the Miocene Monterey Formation at El Capitan State Beach, California, USA: Journal of Sedimentary Research, v. 72, p. 252–267.

John, C.M., Mutti, M., and Adatte, T., 2003, Mixed carbonate siliciclastic record on the north African margin (Malta)—Coupling of weathering processes and mid-Miocene climate: Geological Society of America Bulletin, v. 115, p. 217–229, doi: 10.1130/0016-7606(2003)1152.0.CO;2.

Johnson, K.M., and Grimm, K.A., 2001, Opal and organic carbon in laminated diatomaceous sediments: Saanich Inlet, Santa Barbara Basin and the Miocene Monterey Formation: Marine Geology, v. 174, p. 159–175, doi: 10.1016/S0025-3227(00)00148-1.

Kazakov, A.V., 1937, The phosphate facies: Origin of phosphorites and geological factors of deposit formation: Proceedings of the Scientific Institute of Fertilizers and Insectofungicides, v. 145, p. 1–106.

Keller, M.A., and Isaacs, C.M., 1985, An evaluation of temperature scales for silica diagenesis in diatomaceous sequences including a new approach based on the Miocene Monterey Formation, California: Geo-Marine Letters, v. 5, p. 31–35.

Khan-Omarzai, S., Coe, R.S., and Barron, J.A., 1993, Magnetostratigraphy: A powerful tool for high-resolution age-dating and correlation in the Miocene Monterey Formation of California: Results from Shell Beach section, Pismo Basin, *in* Aissaoui, D.M., McNeill, D.F., and Hurley, N.F., eds., Applications of Paleomagnetism to Sedimentary Geology: Society of Economic Petrologists and Paleontologists Special Publication 9, p. 95–111.

Khan-Omarzai, S., Coe, R.S., and Barron, J.A., 2001, Paleomagnetism of the middle-upper Miocene Monterey Formation, Shell Beach, Pismo Basin: Implications for the age and origin of the Monterey Formation and tectonic block rotation in central coastal California, *in* Prothero, D.R., ed., Magnetic Stratigraphy of the Pacific Coast: Society of Sedimentary Geology, Pacific Section, Book 91, p. 302–334.

Kleinpell, R.M., 1938, Miocene Stratigraphy of California: Tulsa, Oklahoma, American Association of Petroleum Geologists, 450 p.

Kleinpell, R.M., 1980, Miocene Stratigraphy of California Revisited: American Association of Petroleum Geologists, Studies in Geology, v. 11, 349 p.

Kolodny, Y., and Garrison, R.E., 1994, Sedimentation and diagenesis in paleo-upwelling zones of epeiric and basional settings: A comparison of the Cretaceous Mishash Formation of Israel and the Miocene Monterey Formation of California, *in* Iijima, A., Abed, A.M., and Garrison, R.E., eds., Siliceous, Phosphatic, and Glauconitic Sediments of the Tertiary and Mesozoic: 29th International Geological Congress, Proceedings, Part C: Zeiste, The Netherlands, VSP International, p. 133–158.

Kübler, B., 1983, Dosage quantitatif des minéraux majeurs des roches sédimentaires par diffraction X: Institut de Géologie de Neuchâtel, Cahier, Série ADX, v. 1, 12 p.

Kunitomi, D.S., Hopps, T.E., and Galloway, J.M., eds., 1998, Structure and Petroleum Geology, Santa Barbara

Channel, California: American Association of Petroleum Geologists, Pacific Section, and Coast Geological Society Miscellaneous Publication 46, 328 p.

Lamboy, M., 1994, Nannostructure and genesis of phosphorites from ODP Leg 112, the Peru margin: Marine Geology, v. 118, p. 5–22, doi: 10.1016/0025-3227(94)90110-4.

MacKinnon, T.C., 1989, Petroleum geology of the Monterey Formation in the Santa Maria and Santa Barbara coastal and offshore areas, *in* MacKinnon, T.C., ed., Oil in the California Monterey Formation: 28th International Geological Congress, American Geophysical Union, Fieldtrip Guidebook T311, p. 11–27.

Malone, M.J., Baker, P.A., and Burns, S.J., 1994, Recrystallization of dolomite: Evidence from the Monterey Formation (Miocene), California: Sedimentology, v. 41, p. 1223–1239.

Medrano, M.D., and Piper, D.Z., 1997, Fe-Ca-phosphate, Fe-silicate, and Mn-oxide minerals in concretions from the Monterey Formation: Chemical Geology, v. 138, p. 9–23, doi: 10.1016/S0009-2541(96)00170-2.

Mirtov, Y., Zanin, Y., Krasilnikova, N.A., Gurevich, B.G., Krivoputskaya, L.M., Krasilnikova, I.G., and Sukhov, Y.K.M., 1987, Ultramicrostructures of phosphorites: Transactions of the Institute of Geology and Geophysics, Siberian Branch of the Academy of Sciences of the USSR, Nauka, Moscow, v. 670, 224 p.

Müller, P.J., and Suess, E., 1979, Productivity, sedimentation rate, and sedimentary organic matter in the oceans—I. Organic carbon preservation: Deep Sea Research, v. 26A, p. 1347–1362.

Murata, K.J., and Randall, R.G., 1975, Silica mineralogy and structure of the Monterey Shale, Temblor Range, California: U.S. Geological Survey Journal of Research, v. 3, p. 567–572.

Mutti, M., Bernoulli, D., and Stille, P., 1997, Temperate carbonate platform drowning linked to Miocene oceanographic events: Maiella platform margin, Italy: Terra Nova, v. 9, p. 122–125.

Ozalas, K., Savrda, C.E., and Fullerton, R.R., 1994, Bioturbated oxygenation-event beds in siliceous facies: Monterey Formation (Miocene), California: Palaeogeography, Palaeoclimatology, Palaeoecology, v. 112, p. 63–83, doi: 10.1016/0031-0182(94)90134-1.

Pagani, M., Arthur, M.A., and Freeman, K.H., 1999, Miocene evolution of atmospheric carbon dioxide: Paleoceanography, v. 14, p. 273–292, doi: 10.1029/1999PA900006.

Pearson, P.N., and Palmer, M.R., 2000, Atmospheric carbon dioxide concentrations over the past 60 million years: Nature, v. 406, p. 695–699, doi: 10.1038/35021000.

Piper, D.Z., and Isaacs, C.M., 2001, The Monterey Formation–bottom water redox and photic zone primary productivity, *in* Isaacs, C.M., and Rullkötter, J., eds., The Monterey Formation: From Rocks to Molecules: New York, Columbia University Press, p. 31–58.

Pisciotto, K.A., 1981, Diagenetic trends in siliceous facies of the Monterey Formation in the Santa Maria region, California: Sedimentology, v. 28, p. 547–571.

Pisciotto, K.A., and Garrison, R.E., 1981, Lithofacies and depositional environments of the Monterey Formation, California, *in* Garrison, R.E., and Douglas, R.G., eds., The Monterey Formation and related siliceous rocks of California: Society of Economic Petrologists and Paleontologists, Pacific Section, Special Publication 15, p. 97–122.

Raymo, M.E., 1994, The Himalayas, organic carbon burial, and the climate in the Miocene: Paleoceanography, v. 9, p. 399–404, doi: 10.1029/94PA00289.

Raymo, M.E., and Ruddiman, W.F., 1992, Tectonic forcing of late Cenozoic climate: Nature, v. 359, p. 117–122.

Raymo, M.E., Ruddiman, W.F., and Roelich, P.N., 1988, Influence of late Cenozoic mountain building on ocean geochemical cycles: Geology, v. 16, p. 649–653.

Reimers, C., and Suess, E., 1983, Spatial and temporal patterns of organic matter accumulation on the Peru continental margin, *in* Thiede, J., and Suess, E., eds., Coastal Upwelling: Its Sediment Record, part B: New York, Plenum Press, p. 311–345.

Reimers, C., Kastner, M., and Garrison, R.E., 1990, The role of bacterial mats in phosphate mineralization with particular reference to the Monterey Formation, *in* Burnett, W.C., and Riggs, S.R., eds., Phosphate Deposits of the World, vol. 3, Neogene to Modern Phosphorites: Cambridge, Cambridge University Press, p. 300–311.

Retallack, G.J., 2001, Cenozoic expansion of grasslands and climatic cooling: Journal of Geology, v. 109, p. 407–426, doi: 10.1086/320791.

Riggs, S.R., 1979, Phosphorite sedimentation in Florida—A model phosphogenic system: Economic Geology and the Bulletin of the Society of Economic Geologists, v. 74, p. 285–314.

Riggs, S.R., 1984, Paleoceanographic model of Neogene Phosphorite deposition, U.S. Atlantic continental margin: Science, v. 223, p. 123–131.

Riggs, S.R., and Sheldon, R.P., 1990, Paleoceanographic and paleoclimatic controls of the temporal and geographic distribution of Upper Cenozoic continental margin phosphorites, *in* Burnett, W.C., and Riggs, S.R., eds., Phosphate deposits of the world: Vol. 3, Genesis of Neogene to Recent Phosphorites: Cambridge, New York, Cambridge University Press, p. 207–222.

Ruttenberg, K.C., 1992, Development of a sequential extraction method for different forms of phosphorus in marine sediments: Limnology and Oceanography, v. 37, p. 1460–1482.

Schlager, W., 1981, The paradox of drowned reefs and carbonate platforms: Geological Society of America Bulletin, v. 92, p. 197–211.

Schuffert, J.D., Jahnke, R.A., Kastner, M., Leather, J., Sturz, A., and Wing, M.R., 1994, Rates of formation of modern phosphorite off western Mexico: Geochimica et Cosmochimica Acta, v. 58, p. 5001–5010, doi: 10.1016/0016-7037(94)90227-5.

Seilacher, A., 1969, Fault-graded beds interpreted as seismites: Sedimentology, v. 13, p. 155–159.

Shemesh, A., 1990, Crystallinity and diagenesis of sedimentary apatites: Geochimica et Cosmochimica Acta, v. 54, p. 2433–2438, doi: 10.1016/0016-7037(90)90230-I.

Soudry, D., and Lewy, Z., 1988, Microbially influenced formation of phosphate nodules and megafossil moulds (Negev, southern Israel): Palaeogeography, Palaeoclimatology, Palaeoecology, v. 64, p. 15–34, doi: 10.1016/0031-0182(88)90139-3.

Southam, J.R., and Hay, W.W., 1981, Global sedimentary mass balance and sea level changes, *in* Emiliani, C., ed., The Sea: New York, John Wiley & Sons, v. 7, p. 1617–1684.

Stein, R., 1991, Accumulation of organic carbon in marine sediments: Lecture Notes in Earth Sciences: Berlin, Springer, v. 34, 217 p.

Stille, P., Riggs, S., Clauer, N., Ames, D., Crowson, R., and Snyder, S., 1994, Sr and Nd isotopic analysis of phosphorite sedimentation through one Miocene high-frequency depositional cycle on the North Carolina shelf: Marine Geology, v. 117, p. 253–273, doi: 10.1016/0025-3227(94)90019-1.

Stow, D.A.V., Huc, A.Y., and Bertrand, P., 2001, Depositional processes of black shales in deep water: Marine and Petroleum Geology, v. 18, p. 491–498, doi: 10.1016/S0264-8172(01)00012-5.

Summerhayes, C.P., 1981, Oceanographic controls on organic matter in the Miocene Monterey Formation, *in* Garrison, R.E., and Douglas, R.G., eds., The Monterey Formation and Related Siliceous Rocks of California: Society of Economic Petrologists and Paleontologists, Pacific Section, Special Publication 15, p. 213–219.

Tamburini, F., 2001, Phosphorus in marine sediments during the last 150,000 years: Exploring relationships between continental weathering, productivity, and climate [Ph.D. thesis]: Neuchâtel, University of Neuchâtel, 217 p.

Utescher, T., Mosbrugger, V., and Ashraf, A.R., 2000, Terrestrial climate evolution in northwest Germany over the last 25 million years: Palaios, v. 15, p. 430–449.

Van Cappellen, P., 1991, The formation of marine Apatite: A kinetic study [Ph.D. thesis]: New Haven, Yale University, 240 p.

Vincent, E., and Berger, W.H., 1985, Carbon dioxide and polar cooling in the Miocene: The Monterey hypothesis, *in* Sundquist, E.T., and Broecker, W.S., ed., The Carbon Cycle and Atmospheric CO_2, Natural Variations Archean to Present: American Geophysical Union, Geophysical Monographs, v. 32, p. 455–468.

Weissert, H., Lini, A., Föllmi, K.B., and Kuhn, O., 1998, Correlation of early Cretaceous carbon isotope stratigraphy and platform drowning events: A possible link?: Palaeogeography, Palaeoclimatology, Palaeoecology, v. 137, p. 189–203, doi: 10.1016/S0031-0182(97)00109-0.

White, L.D., 1992, Overview of the Monterey Formation, dating techniques, sedimentary components, and paleoceanographic parameters, *in* Schwalbach, J.R., and Bohacs, K.M., eds., Sequence Stratigraphy in fine-grained rocks: Examples from the Monterey Formation: Society of Economic Petrologists and Paleontologists, Pacific Section, Special Publication 70, p. 3–5.

White, L.D., Garrison, R.E., and Barron, J.A., 1992, Miocene intensification of upwelling along the California margin as recorded in siliceous facies of the Monterey Formation and offshore DSDP sites, *in* Summerhayes, C.P., Prell, P., and Emeis, K.C., eds., Upwelling systems: Evolution since the early Miocene: Geological Society [London] Special Publication 63, p. 429–442.

Wignall, P.B., 1994, Black Shales: Oxford Monographs on Geology and Geophysics, v. 30, 127 p.

Woodruff, F., and Savin, S.M., 1989, Miocene deepwater oceanography: Palaeoceanography, v. 4, p. 87–140.

Zachos, J., Pagani, M., Sloan, L., Thomas, E., and Billups, K., 2001, Trends, rhythms, and aberrations in global climate 65 Ma to present: Science, v. 292, p. 686–693, doi: 10.1126/science.1059412.